Bioinspired synthesis of magnetic nanoparticles

by

Anand David

A thesis submitted to the graduate faculty

in partial fulfillment of the requirements for the degree of

MASTER OF SCIENCE

Major: Chemical Engineering

Program of Study Committee:
Balaji Narasimhan, Major Professor
Surya K. Mallapragada
Mufit Akinc

Iowa State University

Ames, Iowa

2009

TABLE OF CONTENTS

ACKNOWLEDGEMENTS

I would like to thank Dr. Balaji Narasimhan and Dr. Surya K. Mallapragada for their guidance of my research project. I would also like to thank Dr. Mufit Akinc for serving on my Program of Study committee. I would also like to thank Dr. Tanya Prozorov for her guidance and training that has been of great benefit to me, in addition to her many hours of microscopy work to obtain TEM images for me. I also want to acknowledge Dr. Soenke Seifert for his assistance in SAXS measurements and analysis. In addition, I acknowledge the Department of Energy Basic Energy Sciences for funding my research.

CHAPTER 1. INTRODUCTION

1.1 Introduction

The synthesis of magnetic nanoparticles has long been an area of active research [1-3]. Magnetic nanoparticles can be used in a wide variety of applications such as magnetic inks, magnetic memory devices, drug delivery, magnetic resonance imaging (MRI) contrast agents, and pathogen detection in foods. In applications such as MRI, particle uniformity is particularly crucial, as is the magnetic response of the particles. Uniform magnetic particles with good magnetic properties are therefore required [4]. One particularly effective technique for synthesizing nanoparticles involves biomineralization, which is a naturally occurring process that can produce highly complex nanostructures. Also, the technique involves mild conditions (ambient temperature and close to neutral pH) that make this approach suitable for a wide variety of materials [5].

The term “bioinspired” is important because biomineralization research is inspired by the naturally occurring process, which occurs in certain microorganisms called “magnetotactic bacteria.” Magnetotactic bacteria use biomineralization proteins to produce magnetite crystals having very good uniformity in size and morphology [6]. The bacteria use these magnetic particles to navigate according to external magnetic fields [7, 8]. Because these bacteria synthesize high quality crystals, research has focused on imitating aspects of this biomineralization in vitro. In particular, a biomineralization iron-binding protein found in a certain species of magnetotactic bacteria, magnetospirillum magneticum, AMB-1, has been extracted and used for in vitro magnetite synthesis; Pluronic F127 gel was used to increase

the viscosity of the reaction medium to better mimic the conditions in the bacteria. It was shown that the biomineralization protein mms6 was able to facilitate uniform magnetite synthesis [4]. In addition, a similar biomineralization process using mms6 and a shorter version of this protein, C25, has been used to synthesize cobalt ferrite particles [9].

The overall goal of this project is to understand the mechanism of magnetite particle synthesis in the presence of the biomineralization proteins, mms6 and C25. Previous work has hypothesized that the mms6 protein helps to template magnetite and cobalt ferrite particle synthesis and that the C25 protein templates cobalt ferrite formation [4, 9]. However, the effect of parameters such as the protein concentration on the particle formation is still unknown. It is expected that the protein concentration significantly affects the nucleation and growth of magnetite. Since the protein provides iron-binding sites, it is expected that magnetite crystals would nucleate at those sites. In addition, in the previous work, the reaction medium after completion of the reaction was in the solution phase, and magnetic particles had a tendency to fall to the bottom of the medium and aggregate. The research presented in this thesis involves solid Pluronic gel phase reactions, which can be studied readily using small-angle x-ray scattering, which is not possible for the solution phase experiments. In addition, the concentration effect of both of the proteins on magnetite crystal formation was studied.

1.2. Applications of Magnetic Nanoparticles

Magnetic nanoparticles can be used to enhance the contrast of the MRI image by localizing the particles at the region in the body of interest. By attaching tumor-specific antigens or other antibodies to magnetic particles, tumor detection is possible (Figure 1.1) [10].

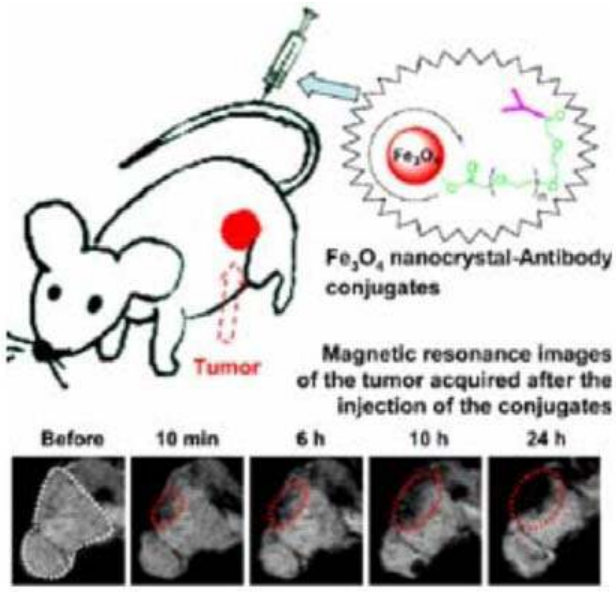

Figure 1.1. Magnetite particles with conjugated antibodies specific to a tumor are injected into the blood stream of a rodent model. The particles accumulate at the site of the tumor. MRI images show the particle accumulation over time [10].

In addition to the antigen providing tumor-specific binding, magnetic particles can be transported using an external magnetic field gradient [11, 12]. The particles need to be able to fit into blood vessels and be highly magnetic so that they can be steered by the external magnetic fields to the desired location. In addition, they need to be non-toxic and non-immunogenic [13]. Transport of the magnetic particles to the desired location can be impeded by macrophages or the reticulo endothelial system, so the particles can be coated with

hydrophilic polymers such as poly(ethylene glycol) [14]. Another example of contrast improvement using magnetic particles is in MRI of the brain (Figure 1.2) [15].

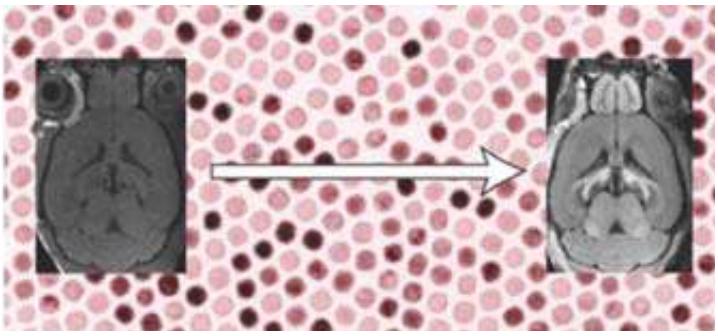

Figure 1.2. Magnetic manganese (II) oxide (MnO) nanoparticles used to improve the contrast of an MRI brain image [15].

The magnetic particles act as contrast agents by causing a disturbance of the magnetic field applied in the area that they are localized. MRI typically uses nuclear magnetic resonance (NMR) signals from hydrogen nuclei of water molecules. The disturbance in the magnetic field changes the radio frequency of the NMR signals [16]. Magnetite particles have already been used to enhance MRI and are advantageous because of their biocompatibility and ability to be functionalized readily [17].

Another application of magnetic nanoparticles is in the detection of pathogens in foods. An advantage of using magnetic nanoparticles for pathogen detection is their high surface area for attachment and excellent adsorption ability [18, 19]. In addition, the particles can rapidly agglomerate or go back into the food stream as a result of changes in an external magnetic field [20]. For detection of pathogens using magnetic particles, antibodies that are specific to the pathogens that need to be detected must be present. Antibodies would be attached to the magnetic particles using suitable attachment chemistries and could be held onto a surface

using a magnet or another type of external magnetic field according to techniques in the literature. One example is shown in Figure 1.3 [20].

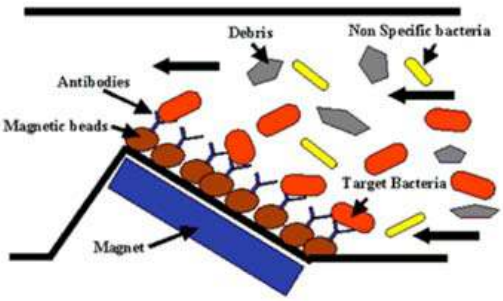

Figure 1.3. Pathogen detection system having antibody complex that binds specific pathogens [20].

Since the surface area of the nanoparticles is very high, there is more area for attachment of antibodies to the magnetic particles, and the pathogen detection sensitivity is enhanced. Thus, extremely low concentrations of food pathogens can be detected [21]. To help improve antibody attachment, a few atomic layers of polymer (either natural or synthetic), oxide surfaces (silica or alumina), or inorganic metal can be coated on the magnetic particles [22, 23]. Another way to facilitate attachment is by functionalizing the particle with ionic groups. For example, negatively charged groups can be coated on magnetite particles by using a surfactant such as sodium oleate (Figure 1.4) [24].

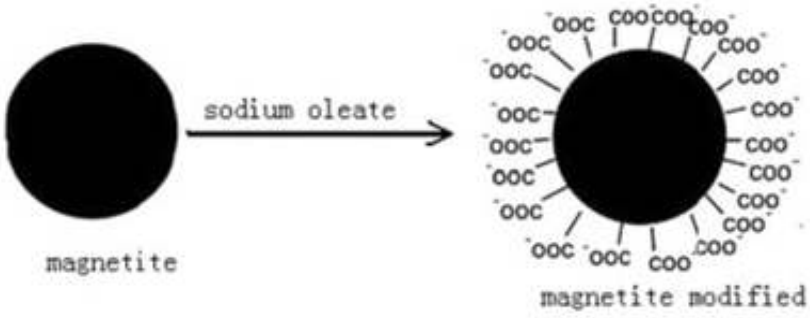

Figure 1.4. Ionic modification of magnetite using a surfactant [24].

The food stream can be passed over the surface, and pathogens specific for the antibodies bound to the particles will attach to the antibodies, as shown in Figure 1.3. The magnet can then be removed, and the magnetic particles with bound antibodies and pathogens can be eluted for analysis [20].

Magnetic sensors employing magnetic particles can be used for detection of individual biological pathogens [21]. In order for detection of single pathogen molecules, the magnetic particles used need to be uniform in size and morphology and have high magnetic moments [25]. One method of detecting the pathogens after elution of the magnetic particles with bound antibodies and pathogens is by using giant magneto-resistive (GMR) sensors. GMR sensors are very sensitive to even small magnetic fields, with large signal-to-noise ratios (SNR) when magnetic nanoparticles are used [26].

In addition to MRI and pathogen detection, magnetic particles have a vast number of other applications. The particles can be used for drug delivery and targeting [4]. Also, external magnetic fields can be used to heat the particles so that they can be used as hyperthermia agents to treat cancerous tumors [11]. In addition, magnetic particles can be used in an immunoassay system that detects human insulin levels [27].

Chapter 2 provides a summary of the literature that is relevant for the magnetite work described in this thesis. Chapter 3 summarizes the goals of this research project. Chapter 4 describes the solid-phase experiments and the characterization of the nanoparticles using small angle X-ray scattering and what may be learned from these studies about the

mechanism of magnetite synthesis. Chapter 5 summarizes the main conclusions of the work and discusses future areas of research in this field.

1.3. References

1. Malaiya, A.; Vyas, S. P. Preparation and characterization of indomethacin magnetic nanoparticles. *Journal of Microencapsulation*. **1988**, 5 (3), 243-53.

2. Ibrahim, A.; Couvreur, P.; Roland, M.; Speiser, P. Magnetic nanoparticles for targeting of drugs. Expo. - Congr. Int. Technol. Pharm., 3rd. **1983**, 4, 180-4.

3. Schroeder, U.; Mosbach, K. Intravascularly administrable, magnetically responsive nanosphere or nanoparticle. PCT Int. Appl. **1983**, 15 pp.

4. Prozorov, T.; Mallapragada, S. K.; Narasimhan, B.; Wang, L.; Palo, P.; Nilsen-Hamilton, M.; Williams, T. J.; Bazylinski, D. A.; Prozorov, R.; Canfield, P. C. Protein-Mediated Synthesis of Uniform Superparamagnetic Magnetite Nanocrystals. *Adv. Funct. Mater.* **2007**, *17*, 951–957.

5. Amemiya, Y.; Arakaki, A.; Staniland, S.S.; Tanaka, T.; Matsunaga, T. Controlled formation of magnetite crystal by partial oxidation of ferrous hydroxide in the presence of recombinant magnetotactic bacterial protein Mms6. *Biomaterials*. **2007**, 28, 5381-5389.

6. Bazylinski, D. A.; Frankel, R. B. Magnetosome Formation in Prokaryotes. *Nat. Rev. Microbiol.* **2004**, *2*, 217–230.

7. Bellini, S. J. About a Unique Behavior of Freshwater Bacteria. *Instit. Microbiol.* **1963**, http://www.calpoly.edu/~rfrankel/SBellini1.pdf. Cal Poly. (accessed April 21, 2009).

8. Blakemore, R. Magnetotactic Bacteria. *Science*. **1975**, 190, 377-379.

9. Prozorov, T.; Palo, P.; Wang, L.; Nilsen-Hamilton, M.; Jones, D.; Orr, D.; Mallapragada, S.K.; Narasimhan, B.; Canfield, P.C.; Prozorov, R. Cobalt ferrite nanocrystals: outperforming magnetotactic bacteria. *ACS Nano*. **2007**, 1, 228–233.

10. Gov.cn, "Study reveals potential MRI contract agent for tumor detection." http://english.gov.cn/2006- 12/05/content_461502.htm (accessed August 19, 2008).

11. Pankhurst, Q. A.; Connolly, J.; Jones, S. K.; Dobson, J. Applications of magnetic nanoparticles in biomedicine. *J. Phys. D: Appl. Phys.* **2003**, *36*, R167–R181.

12. Simonite, T. http:// technology.newscientist.com/channel/tech/dn11412-mri-scanner-steers- magnetic-particle-in-live-animals- blood.html. New Scientist Tech. (accessed August 16, 2008).

13. Tartaj, P.; del Puerto Morales, M.; Veintemillas-Verdaguer, S.; Gonzalez-Carreno, T.; Serna, C. J. The preparation of magnetic nanoparticles for applications in biomedicine. *J. Phys. D: Appl. Phys.* **2003**, 36, R182.

14. Gupta, A. K.; Gupta, M. Synthesis and surface engineering of iron oxide nanoparticles for biomedical applications. *Biomaterials*. **2005**, 26, 3995–4021.

15. Hyeon, T. The path of chemistry in Korea. *Nature Materials*. **2007**, 6, 541-543.

16. Bowtell, R. A colourful future for MRI. *Nature*. **2008**, 453, 993-994.

17. Wang, X.; Zhang, R.; Wu, C.; Dai, Y.; Song, M.; Gutmann, S.; Gao, F.; Lv, G.; Li, J.; Li, X.; Guan, Z.; Fu, D.; Chen, B. The application of Fe3O4 nanoparticles in cancer research: A new strategy to inhibit drug resistance. *J. Biomed. Mater. Res. A.* **2007**, *80*, 852.

18. Hsing, I.; Xu,Y.; Zhao, W. Micro- and nano- magnetic particles for applications in biosensing. *Electroanalysis*. **2007**, 19, 755- 768.

19. Kaushik. A.; Khan, R.; Solanki, P. R.; Pandey, P.; Alam, J.; Ahmad, S.; Malhotra, B. D. Iron oxide nanoparticles-chitosan composite based glucose biosensor. *Biosensors and Bioelectronics*, In Press, Corrected Proof, **2008**, Epub. ahead of print.

20. Food Processing Technology (SPG Media Limited), "Pathatrix Pathogen Testing System." http://www.foodprocessingtechnology.com/projects/cadburypathatix/ (accessed August 16, 2008).

21. Sandhu, A. New probes offer much faster results. *Nature Nanotechnology*. **2007**, 2, 746-748.

22. Gupta, A. K.; Gupta, M. Synthesis and surface engineering of iron oxide nanoparticles for biomedical applications. *Biomaterials,* **2005**, *26*, 3995.

23. Wan, S.; Huang, J.; Guo, M.; Zhang, H.; Cao, Y.; Yan, H.; Liu, K. Biocompatible superparamagnetic iron oxide nanoparticle dispersions stabilized with poly(ethylene glycol)– oligo(aspartic acid) hybrids *J. Biomed. Mater. Res.* **2007**, *80A*, 946-954.

24. Sun, J.; Zhou, S.; Hou, P.; Yang, Y.; Weng, J.; Li, X.; Li, M. Synthesis and characterization of biocompatible Fe3O4 nanoparticles. *J. Biomed. Mater. Res. A.* **2007**, 80A (2), 333-341.

25. Robinson, D. B.; Persson, H. H.; Zeng, H.; Li, G.; Pourmand, N.; Sun, S.; Wang, S. X. DNA-Functionalized MFe2O4 (M= Fe, Co, or Mn) Nanoparticles and Their Hybridization to DNA-Functionalized Surfaces. *Langmuir.* **2005**, *21*, 3096-3103.

26. de Boer, B. M.; Kahlman, J. A. H. M.; Jansen, T. P. G. H.; Duric, H.; Veen, J. An integrated and sensitive detection platform for magneto-resistive biosensors. *Biosens. Bioelectron.* **2007**, 22, 2366–2370.

27. Matsunaga, T.; Sakaguchi, T.; Okamura, Y. Molecular and Biotechnological Aspects of Bacterial Magnetite. In *Biomineralization: Molecular and Biotechnological Aspects of Bacterial Magnetite*, 2nd ed.; Bäuerlein, E., Ed.; Wiley-VCH: **2005**; pp. 103-104.

CHAPTER 2. BACKGROUND AND LITERATURE REVIEW

2.1. Summary

This chapter gives a summary of the literature that is relevant for the magnetite work described in this thesis. Section 2.2 provides an introduction to bioinspired synthesis pathways involving biomineralization for nanoparticle synthesis. Section 2.3 explains the discovery of magnetotactic bacteria, and Section 2.4 discusses how the magnetotactic bacteria synthesize magnetite particles. Section 2.5 explains how the biomineralization process in the bacteria has been mimicked for in vitro synthesis, while Section 2.6 shows how some other processes compare with the bioinspired approach of synthesis. Section 2.7 focuses on how the bioinspired approach can facilitate production of nanoparticles of different magnetic materials. Section 2.8 concludes the chapter with a discussion of some literature pertaining to magnetic particles.

2.2. Biomineralization Synthesis Pathway for Nanoparticles

Many approaches exist for producing nanoparticles [1- 4]. One of the most intriguing involves bioinspired synthesis pathways. Pathways found in nature can inspire in vitro synthesis pathways that attempt to mimic the natural processes. One of the most intriguing bioinspired pathways is that of biomineralization [5]. Biomineralization involves the used of organic molecules for nucleation and growth of crystals at ambient temperature and close to neutral pH [6]. Nanoparticle crystals nucleate and grow in size in supersaturated solution from ions and molecules [7]. The main advantage of biomineralization compared to other

synthetic processes is the mild temperature and pH. Another advantage is that there is no requirement for organic solvents. Whereas other processes such as thermal decomposition require high temperatures and the use of organic solvents, biomineralization provides a pathway for formation of magnetic particles in aqueous environments. Because of these advantages, much research has been conducted to study the biology and chemistry involved in natural biomineralization processes in order to imitate them using in vitro synthesis techniques [6].

Two main types of natural biomineralization involve calcification and silicification. The mechanism of biomineralization is not completely understood. In both calcification and silicifation, it is thought that organic macromolecules that are genetically controlled act to cause formation of organic-inorganic nanoparticles. Then, they act as templates to assemble micro- to macro architectures with complex patterns [8]. The macromolecules therefore function as structure-directing agents [9]. The macromolecules are reabsorbed, leaving the inorganic part intact [8].

There are many examples involving imitation of biomineralization in the laboratory. One involves the synthesis of zinc oxide particles. Zinc oxide is nontoxic and biocompatible and can be used in many different applications such as dental implants and light-emitting diodes [10-13]. One biomineralization pathway for producing zinc oxide involves using a silk

fibroin (SF) peptide that acts as a template for particle synthesis. This peptide induces nucleation of the particles and also affects their morphology [10].

Another example involves the use of biomineralization in bone tissue engineering. For mechanical implants, there is often mismatch between the implant and the natural environment in which the implant is placed. Synthetic techniques can imitate the self-assembly process of bone growth [14, 15]. In nature there are a number of peptide motifs that aid self-assembly [14]. An example of biomineralization to aid bone growth involves the use of a chimeric protein hydrogel; the protein nucleates hydroxyapatite [6, 7, 16]. The apatites are highly oriented, similar to natural bone mineral [14].

Another example of biomineralization is the crystallization of calcium carbonate. Calcium carbonate crystals exemplify what biomineralization is capable of, namely the formation of three-dimensional single crystals having well-defined structures. In addition, for the case of calcium carbonate, there can be well defined crystal orientations. An example in nature of well defined calcium carbonate is in calcite skeletal plates of coccoliths and echinoderms. These nature phenomena have inspired research that attempts to produce these crystals in vitro. As an example, the introduction of amorphous calcium carbonate into a template of polymer spheres leads to the formation of calcium carbonate crystals with controlled orientation. In addition, patterning exists down to the nano-scale in this bioinspired research [17].

2.3. Discovery of Magnetotactic Bacteria

Magnetotactic bacteria were first discovered in 1958 by Salvatore Bellini, who noted that in freshwater that there were microorganisms which always seemed to travel in the same direction [18, 19]. Bellini inspected the organisms under a microscope, changing environment conditions, but that did not seem to affect the persistent movement of the microorganisms in one direction. Bellini noted that the organisms always traveled toward the North Pole, which was the direction that the organisms were affected by magnetic attraction, as shown by Bellini when he used a strong magnet to "steer" the bacteria [19].

Bellini was not the first to coin the term "magnetotactic bacteria" for these microorganisms. This term was designated by James Blakemore, who in the 1970s made some interesting observations of these bacteria. He noted that they possess flagella and contained "novel structured particles, rich in iron." Blakemore postulated that these particles impart a magnetic moment to the bacteria that aid in the movement of the bacteria [20].

2.4. Synthesis of Magnetite in Magnetotactic Bacteria

Since the work of Bellini and Blakemore, the research community's understanding of magnetotactic bacteria has grown significantly. Magnetotactic bacteria produce intracellular structures called magnetosomes. Each magnetosome contains a magnetite crystal surrounded by a lipid bilayer. Magnetosomes tend to align in chains inside the bacteria as the magnetic moments of the individual magnetite particles align with one another (Figure 2.1) [21].

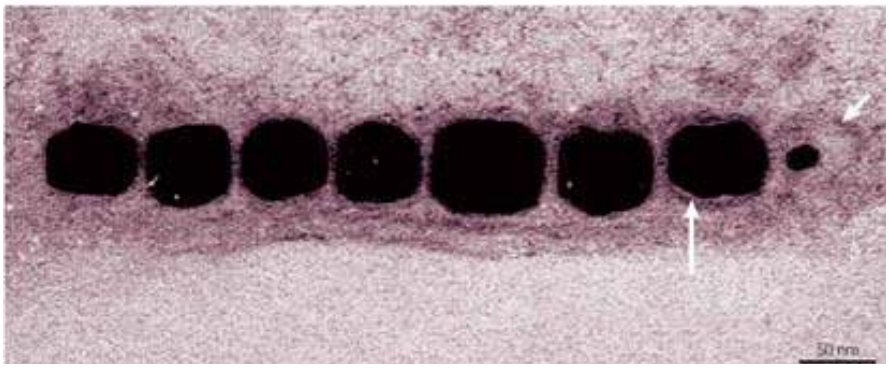

Figure 2.1. Magnetosome chain inside magnetotactic bacteria. Note the magnetosome membranes indicated by the white arrows. Also note the growing magnetite crystal on the right side [21].

The net magnetic moment of each chain equals the sum of the individual magnetic moments [21]. Magnetotactic bacteria use these magnetosomes to orient themselves in responses to external magnetic fields, including the earth's magnetic field [20]. Different types of bacteria make magnetite crystals with a variety of morphologies and may contain one or more magnetosome chains (Figure 2.2) [22].

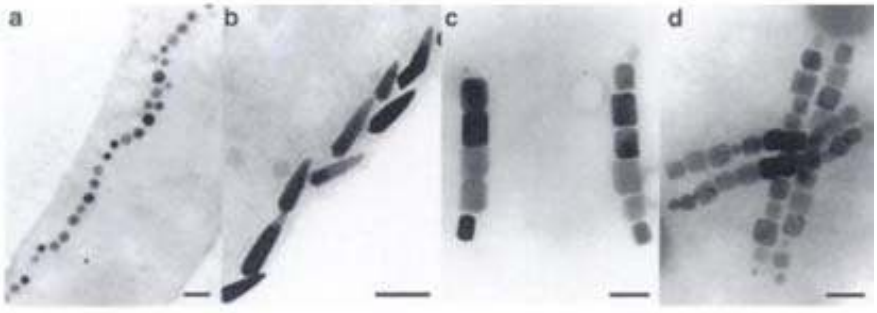

Figure 2.2. Examples of the variety of magnetosome chains and magnetite particles synthesized by different types of magnetotactic bacteria [22].

The magnetosome membrane is made up of phospholipids and fatty acids as well as some proteins that resemble cytoplasmic membrane proteins. This may suggest that the magnetosome membrane vesicle is formed when a portion of the cytoplasmic membrane folds and pinches off. The exact mechanism by which the magnetite is formed in the magnetosome is still unknown [4]. A proposed mechanism is that ferric ions (Fe^{3+}) are reduced on the surface of the cell, transported into the cytoplasm, transported into the magnetosome vesicle, and then oxidized to produce magnetite. The formation of the magnetite crystals in the vesicles is thought to be aided by proteins that are bound to the crystals [23]. These proteins are in some way involved in a biomineralization process that facilitates magnetite formation. Biomineralization involves the use of organic molecules for nucleation and growth of crystals at ambient temperature and close to neutral pH [6]. Biomineralization facilitates the formation of uniform magnetite crystals by magnetotactic bacteria [6, 23, 24].

One of the types of magnetotactic bacteria that synthesize magnetite crystals is Magnetospirillum magneticum strain, AMB-1. In these bacteria, it has been found that several proteins, designated as mms5, mms6, mms7, and mms13, are bound to the magnetite crystals. All of these proteins have hydrophobic N-terminal and hydrophilic C-terminal regions. The hydrophilic C-terminal region has hydroxyl and carboxyl groups that bind iron ions [23].

2.5. In Vitro Synthesis of Magnetite using His-mms6

Because uniformity in size and shape is desired and is provided by the biomineralization process of magnetite formation, in vitro synthetic attempts have been made to mimic the biomineralization process found in magnetotactic bacteria. One such attempt involves mimicking the process found in magnetospirillum magneticum AMB-1. In these magnetotactic bacteria, the four proteins mms5, mms6, mms7, and mms13 bind to magnetite crystals - so it was thought that these proteins help in magnetite formation. One of these proteins, mms6, was chosen, although the others could have been as well. Along with this protein, Pluronic F127, a triblock copolymer, was used to slow down diffusion rates of reagents and provide a high viscosity similar to that found in the bacteria. The ability of the mms6 protein to facilitate magnetite production in vitro was studied [25]. $FeCl_2/FeCl_3$ mixtures were reacted with NaOH to form magnetite according to the following reaction:

$$FeCl_2 + 2FeCl_3 + 8NaOH \rightarrow Fe_3O_4 + 8NaCl + 4H_2O$$

An undesired side reaction involved the oxidation of magnetite to hematite [26]:

$$4\ Fe_3O_4 + O_2 \rightarrow 6Fe_2O_3$$

Synthesis of uniform, unoxidized magnetite nanoparticles required carefully controlled anaerobic conditions in which particle growth was slowed down dramatically. Anaerobic conditions were achieved by thorough degassing of the reagents and by the addition of argon to the reaction vessels. The surface area of the nanoparticles was high, resulting in easy oxidation of the particles in the presence of small amounts of air [27]. In addition, from the above reaction it can be noted that one mole of oxygen can react with four moles of

magnetite to form six moles of hematite. Therefore, it is necessary to remove even small amounts of oxygen from the reaction medium. The reaction was slowed down by the addition of Pluronic F127, which is a triblock copolymer consisting of polyethylene oxide and polypropylene oxide units [28, 29:

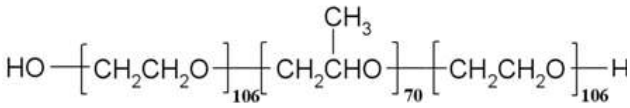

The use of Pluronic F127 raises the viscosity of the reaction medium. Slowing down the diffusion rates is important to approach conditions similar to those in magnetite-producing magnetotactic bacteria. In addition to the anaerobic synthesis with Pluronic, the reaction was further controlled by the addition of the mms6 protein, which mediated the synthesis of the magnetite. The reaction was allowed to proceed for five days. It was found that particles synthesized in the presence of the mms6 protein were of much more uniform size and morphology than those synthesized without it (Figure 2.3) [8].

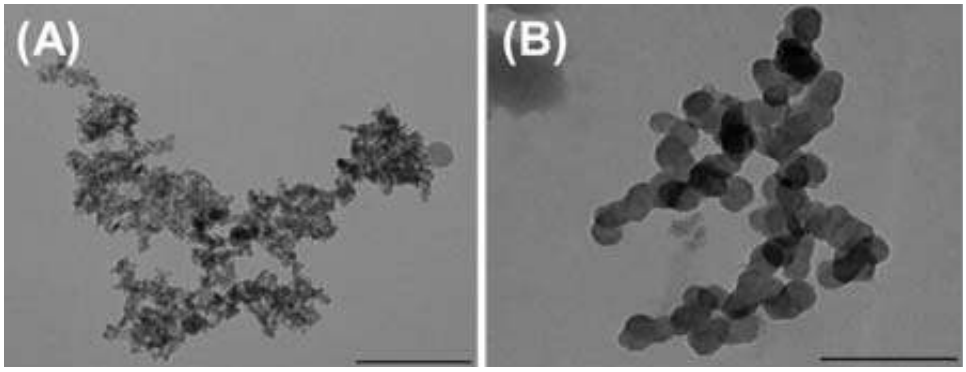

Figure 2.3. TEM pictures of magnetite particles synthesized: A) without mms6 and B) with mms6. Note that the particles in B) have much more uniformity in size and morphology. The scale bars are 200nm in both images [8].

To check if the mms6 protein was able to facilitate uniform particle synthesis in a way other iron-binding proteins cannot, two other proteins, ferritin and His-lcn2, were used for

comparison. However, neither of these iron-binding proteins was able to facilitate the production of uniform particles. This suggests that the templating process was specific to the mms6 protein. In addition, the particles formed using the mms6 protein were found to have superior magnetic properties. It was found that magnetic particles produced using mms6 had higher magnetic moments and higher remanent magnetization, that is, a higher residual magnetization after an external magnetic field was turned off, than the magnetic particles synthesized without the protein (Figures 2.4 and 2.5) [25].

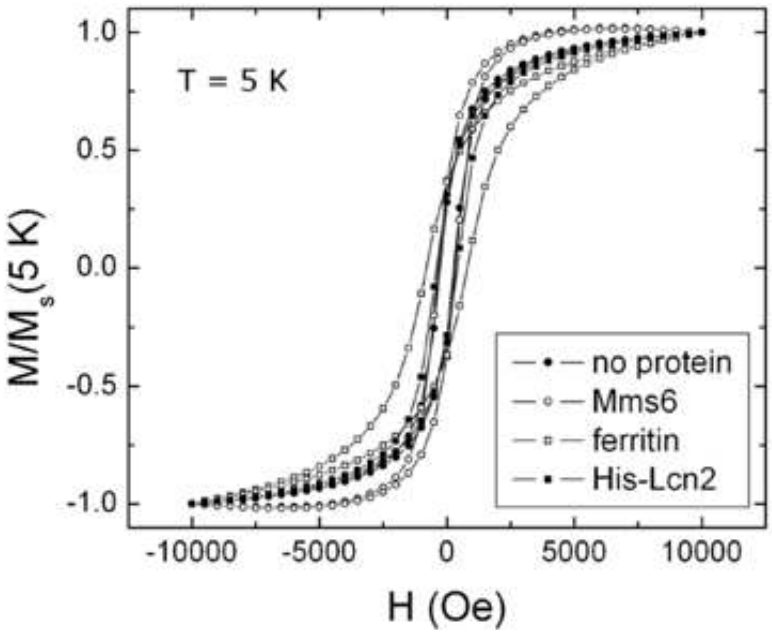

Figure 2.4. Magnetization of different samples at a temperature of 5K as the magnetic field strength is changed. Note that the sample made with the mms6 protein rises to saturation in smaller fields. This is an indicator of a higher magnetic moment per particle. Note that magnetite was also made using two other synthetic proteins, ferritin and His-lcn2, but neither sample had as good magnetic properties as those prepared using mms6 [25].

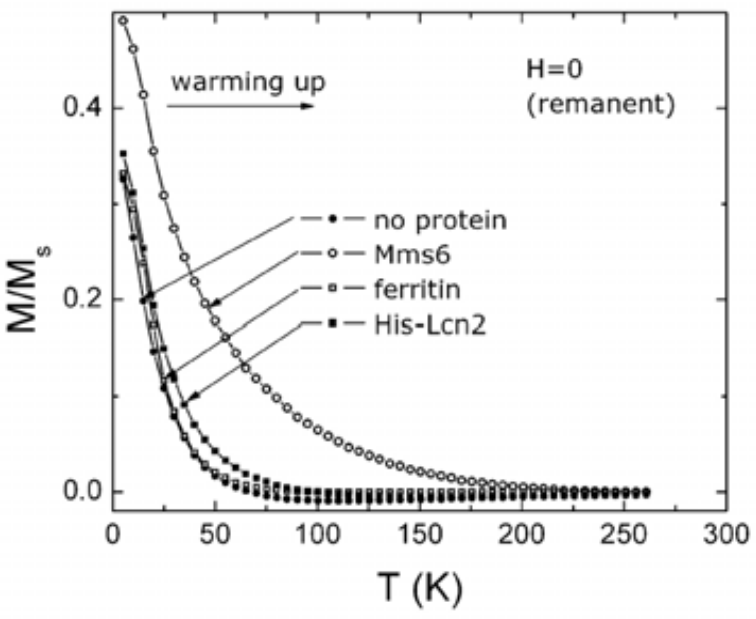

Figure 2.5. Remanent magnetization of samples at different temperatures once the magnetic field was turned off at 5K and the samples slowly heated. Note that the sample made using mms6 shows a higher magnetization up to temperatures as high as 200K [25].

2.6. In Vitro Synthesis of Magnetite Without Biomineralization

It has been shown that biomineralization using mms6 and Pluronic facilitates uniform magnetite crystal formation. There are other processes that do not involve biomineralization that are used to produce magnetite crystals. One involves the reaction of 1,2-hexadecanediol with iron(III) acetylacetonate (Fe(acac)3) in the presence of oleylamine and oleic acid. This is a solution phase reaction requiring temperatures between 200^{o}C and 300^{o}C that results in monodisperse particles [30]. Another process involves the thermal decomposition of iron carboxylate salts to produce uniform magnetite nanoparticles; this process requires a temperature of 320 ^{o}C [31]. An additional process involves reaction of iron(II) acetate, iron(II) acetylacetonate, and iron(III) acetylacetonate with benzyl alcohol to form magnetite

particles. This synthetic scheme is remarkably efficient (synthesis takes one minute). It does use a temperature of 200 ^{o}C and uses microwave radiation for heating [32].

While the above processes are able to facilitate uniform magnetite formation, they all require higher temperatures. This is problematic for multiple reasons. First, higher temperatures require higher energy. Second, even though high temperature processes can be cost-effective, as in the case of using microwave radiation, higher temperatures can limit the applicability of the process to production of those materials that are stable at high temperatures. The biomineralization process is suitable for a much greater variety of materials, including those that are not stable at high temperatures.

2.7. In vitro synthesis of other magnetic nanomaterials

The mms6 protein can facilitate synthesis of high quality magnetite crystals in vitro, but it can also template synthesis of different types of magnetic materials, such as cobalt ferrite ($CoFe_2O_4$), which is not found in magnetotactic bacteria [33]. As part of the cobalt ferrite synthesis, several new methods were employed. One utilized only the iron-binding hydrophilic C-terminal region of the mms6 protein. It was shown that C25-mms6 could be used to enhance synthesis. In addition, the full protein and the short C25-mms6 peptide were covalently attached to Pluronic F127 to provide better control of particle synthesis. It was found that conjugating the proteins to the Pluronic provided better particle morphology and size distribution. In addition, the C25-mms6 peptide was able to provide even better particle synthesis than the full mms6 protein, possibly because the shortened version had less steric

hindrance (Figure 2.6). The conjugated proteins provided particles with better magnetic properties than the unconjugated ones (Figure 2.7).

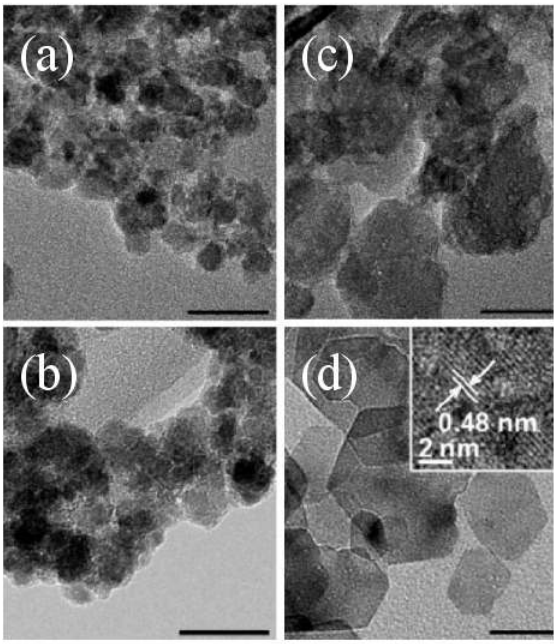

Figure 2.6. TEM of cobalt ferrite particles synthesized: a) with unbound full length mms6 protein, b) with unbound C25 protein, c) with bound full length mms6 protein, and d) with bound C25 protein. The scale bars are 50 nm in all images. The inset in d) is from high resolution TEM and shows the lattice spacing of the central particle in d) [33].

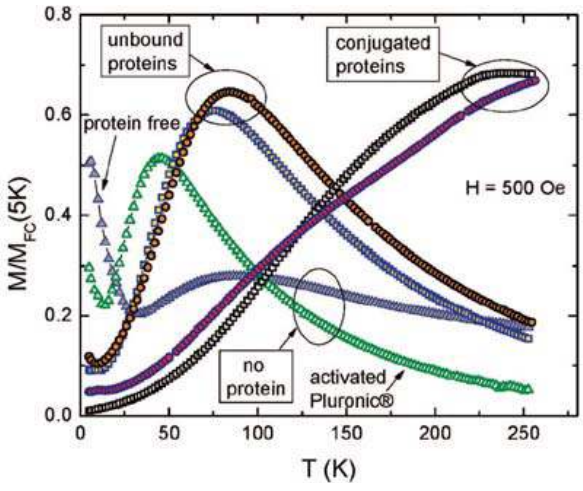

Figure 2.7. Remanent magnetization of cobalt ferrite samples. Note that the samples prepared using conjugated proteins have magnetization values that rise with temperature even past 200K while magnetization values of other samples drop at temperatures less than 100K [33].

2.8. Summary

Biomineralization has been used in a wide variety of nanoparticle syntheses and has inspired our group's synthesis approach because it enables us to synthesize high quality magnetic nanoparticles under mild conditions. In addition, our synthesis approach is suitable for multiple magnetic materials. However, the mechanism of nanoparticle formation in our Pluronic system is largely unknown, so further research has been carried out to better understand the mechanism, as discussed in the rest of this thesis. It is hoped that the contents of this thesis will inspire further efforts to understand the mechanism, use the mechanism to develop improved synthetic techniques, and eventually use the new magnetic particles in applications such as MRI and pathogen detection.

2.9. References

1. Herlin-Boime, N.; Sublemontier, O.; Lacour, F. Synthesis of silicon nanocrystals by laser pyrolysis. *PCT Int. Appl.* **2008**, 36 pp.

2. Baba, K.; Kaneko, T.; Hatakeyama, R. Efficient synthesis of gold nanoparticles using ion irradiation in gas-liquid interfacial plasmas. *Applied Physics Express.* **2009**, 2(3), 035006/1-035006/3.

3. Begum, N. A.; Mondal, S.; Basu, S.; Laskar, R. A.; Mandal, D. Biogenic synthesis of Au and Ag nanoparticles using aqueous solutions of Black Tea leaf extracts. *Colloids and Surfaces, B: Biointerfaces.* **2009**, 71(1), 113-118.

4. Lehtinen K. E. J.; Backman U.; Jokiniemi J. K.; Kulmala M. Three-body collisions as a particle formation mechanism in silver nanoparticle synthesis. *Journal of colloid and interface science.* **2004**, 274 (2), 526-30.

5. Baeuerlein, E., ed.; Behrens, P., ed. Handbook of Biomineralization: Biomimetic and bioinspired chemistry. Wiley-VCH: Weinheim. 2009, back cover introduction.

6. Amemiya, Y.; Arakaki, A.; Staniland, S.S.; Tanaka, T.; Matsunaga, T. Controlled formation of magnetite crystal by partial oxidation of ferrous hydroxide in the presence of recombinant magnetotactic bacterial protein Mms6. *Biomaterials*. **2007**, 28, 5381-5389.

7. Wang, L.; Nancollas, G. H. Pathways to biomineralization and biodemineralization of calcium phosphates : the thermodynamic and kinetic controls. *Dalton Transactions*. **2009**, 15, 2665-2672.

8. Bonucci, E. Calcification and silicification: a comparative survey of the early stages of biomineralization. J Bone Miner Metab. **2009**, 27, 255–264.

9. Gorna, K.; Munoz-Espi, R.; Grohn, F.; Wegner, G. Bioinspired mineralization of inorganics from aqueous media controlled by synthetic polymers. *Macromolecular bioscience*. **2007**, 7 (2), 163-172.

10. Yan, D.; Yin, G.; Huang, Z.; Yang, Mei; L., Xiaoming; Kang, Y.; Yao, Y.; Hao, B.; Han, D. Characterization and Bacterial Response of Zinc Oxide Particles Prepared by a Biomineralization Process. *Journal of Physical Chemistry B.* **2009**, 113 (17), 6047-6053.

11. Zhou, J., Xu, N. S., and Wang, Z. L. Dissolving behavior and stability of ZnO wires in biofluids : a study on biodegradability and biocompatibility of ZnO nanostructures. *Adv. Mater.* **2006,** 18, 2432-2435.

12. Ito M. In vitro properties of a chitosan-bonded hydroxyapatite bone-filling paste. *Biomaterials.* **1991**, 12 (1), 41–5.

13. Tsukazaki, A.; Ohtomo, A.; Onuma, T.; Ohtani, M.; Makino, T.; Sumiya, M.; Ohtani, K.; Chichibu, S. F.; Fuke, S.; Segawa, Yusaburou; Ohno, Hideo; Koinuma, Hideomi; Kawasaki, Masashi. Repeated temperature modulation epitaxy for p-type doping and light-emitting diode based on ZnO. *Nature Materials*. **2005**, 4 (1), 42-46.

14. Gajjeraman, S.; He, G.; Narayanan, K.; George, A. Biological assemblies provide novel templates for the synthesis of biocomposites and facilitate cell adhesion. Advanced Functional Materials. **2008**, 18 (24), 3972-3980.

15. Kumar, M.; Sanford, K. J.; Cuevas, W. P.; Du, M.; Collier, K. D.; Chow, N. Designer Protein-Based Performance Materials. *Biomacromolecules.* **2006**, 7 (9), 2543-2551.

16. Iwatsubo, T.; Sumaru, K.; Kanamori, T.; Shinbo, T.; Yamaguchi, T. Construction of a New Artificial Biomineralization System. *Biomacromolecules*. **2006**, 7 (1), 95-100.

17. Li, C.; Qi, L. Bioinspired fabrication of 3D ordered macroporous single crystals of calcite from a transient amorphous phase. *Angewandte Chemie, International Edition*. **2008**, 47 (13), 2388-2393.

18. Bellini, S. Further studies on "magnetosensitive bacteria." *Instit. Microbiol.* University of Pavia, Italy, **1963**, http://www.calpoly.edu/~rfrankel/SBellini2.pdf. Cal Poly. (accessed May 5, 2009).

19. Bellini, S. J. About a Unique Behavior of Freshwater Bacteria. *Instit. Microbiol.* **1963**, http://www.calpoly.edu/~rfrankel/SBellini1.pdf. Cal Poly. (accessed April 21, 2009).

20. Blakemore, R. Magnetotactic Bacteria. *Science*. **1975**, 190, 377-379.

21. Bazylinski, D. A.; Frankel, R. B. Magnetosome Formation in Prokaryotes. *Nat. Rev. Microbiol.* **2004**, *2*, 217–230.

22. Baeuerlein, E., ed. Biomineralization: Progress in Biology, Molecular Biology, and Application; Wiley-VCH: Weinheim. **2005,** 44, 4833-4834.

23. Arakaki, A.; Webb, J.; Matsunaga, T. A Novel Protein Tightly Bound to Bacterial Magnetic Particles in Magnetospirillum magneticum Strain AMB-1*. *J. Biol. Chem.* **2003**, *278*, 8745–8750.

24. Arakaki, A.; Nakazawa, H.; Nemoto, M; Mori, T.; Matsunaga, T. Formation of magnetite by bacteria and its application. *J. R. Soc. Interface*. **2008**, 5, 977–999.

25. Prozorov, T.; Mallapragada, S. K.; Narasimhan, B.; Wang, L.; Palo, P.; Nilsen-Hamilton, M.; Williams, T. J.; Bazylinski, D. A.; Prozorov, R.; Canfield, P. C. Protein-Mediated Synthesis of Uniform Superparamagnetic Magnetite Nanocrystals. *Adv. Funct. Mater*. **2007**, *17*, 951–957.

26. Forsmo, S.P.E. Oxidation of magnetite concentrate powders during storage and drying, *Int. J. Miner. Process*. **2005,** 75, 135–144.

27. Lu, A.; Salabas, E.L.; Schth F. Magnetic Nanoparticles: Synthesis, Protection, Functionalization, and Application. Angew. *Chem. Int. Edition*, **2007**, 46, 1222-1244.

28. I. Miksık, J.; Charvatova, A.; Eckhardt, Z.; Deyl, *J. Chromatogr*. **2004**, B800, 155.

29. Thiyagarajan, P. Small Angle X-ray and Neutron Scattering: Fundamentals and Applications. Proceedings on the National School on X-ray and Neutron Scattering, Argonne, IL, **2006**; Argonne National Laboratory.

30. Sun, S; Murray, C. B.; Weller, D. K.; Folks, L.; Moser, A. Monodisperse MFe2O4 (M = Fe, Co, Mn) nanoparticles. *Science*. **2000**, 287, 1989–1991.

31. Yu, W. W.; Falkner, J. C.; Yavuz, C. T.; Colvin, V. L. Synthesis of Monodisperse Iron Oxide Nanocrystals by Thermal Decomposition of Iron Carboxylate Salts. *Chem. Commun*. **2004**, 2306–2307.

32. Bilecka, I.; Djerdj, I.; Niederberger, M. One- minute synthesis of crystalline binary and ternary metal oxide nanoparticles, *Chem. Commun.* **2008**, 7, 886-888.

33. Prozorov, T.; Palo, P.; Wang, L.; Nilsen-Hamilton, M.; Jones, D.; Orr, D.; Mallapragada, S.K.; Narasimhan, B.; Canfield, P.C.; Prozorov, R. Cobalt ferrite nanocrystals: outperforming magnetotactic bacteria. *ACS Nano*. **2007**, 1, 228–233.

CHAPTER 3. RESEARCH OBJECTIVES AND ORGANIZATION

3.1 Research Objectives

The overall goal of this project is to understand the mechanism of magnetite formation in the presence of His-mms6 and C25 proteins. Specifically, this work explores the effect of protein concentration on the synthesis of magnetite nanoparticles. This is accomplished by synthesizing magnetite in the solid Pluronic gel medium in the presence of three concentrations of His-mms6 and C25. The effect of the magnetite formation on the Pluronic structure as well as the effect of protein concentration has been studied using small angle X-ray scattering (SAXS).

3.2 Thesis Organization

Chapter 4 presents results of the SAXS studies. Also included is a discussion about TEM images of the magnetite samples (obtained by Dr. Tanya Prozorov) and how they relate to the SAXS results. These results are used to propose some hypotheses that further explain the process of magnetite formation in the presence of His-mms6 and C25 proteins.

CHAPTER 4. MAGNETITE NANOCRYSTAL SYNTHESIS AND CHARACTERIZATION USING BIOMINERALIZATION PROTEINS IN THE SOLID PLURONIC PHASE

4.1. Introduction

Our overall goal is to understand the mechanism of magnetite particle synthesis in the presence of the biomineralization proteins, mms6 and C25. Previous work has hypothesized that the mms6 protein helps template magnetite and cobalt ferrite particle synthesis and that the C25 protein templates cobalt ferrite formation [1, 2]. However, the effect of parameters such as the protein concentration on the nucleation and growth of magnetite particles is still unknown. Since the protein provides iron-binding sites, it is expected that magnetite crystals would nucleate at those sites. In addition, in the previous work, the medium after completion of the reaction was in the solution phase, and magnetic particles had a tendency to fall to the bottom of the medium and aggregate. The current research involves solid Pluronic gel phase reactions, which can be studied readily using small-angle x-ray scattering (SAXS), which is not possible for the solution phase experiments. In addition, the concentration effect of both proteins (i.e., mms6 and C25) on magnetite crystal formation was studied.

4.2. Materials and Methods

4.2.1. Materials

Pluronic F127 NF Prill Poloxamer 407 was purchased from Sigma-Aldrich (St. Louis, MO). $FeCl_2 \cdot 4H_2O$ powder was purchased from Thermo Fisher Scientific (Waltham, MA), while $FeCl_3 \cdot 6H_2O$ powder was obtained from Sigma-Aldrich (St. Louis, MO). Sodium hydroxide was purchased from Fisher Scientific (Fair Lawn, NJ). Buffer consisted of 20mM Tris-HCl and 100mM KCl in filtered water. His-mms6 and C25 proteins were obtained from Lijun Wang and Professor Marit Nilsen-Hamilton (Department of Biochemistry, Biophysics, and Molecular Biology at Iowa State University). Cloning and expression of the mms6 protein is described elsewhere, as is the preparation of the C25 protein [1, 2].

4.2.2. Methods

To study the structure of the Pluronic and how it is influenced by the magnetite, SAXS was used. For these studies, a gel sample is preferred in which the magnetite is dispersed and does not fall to the bottom and aggregate, as is the case at lower Pluronic concentrations. Thus, synthesis experiments were conducted using high concentrations of Pluronic F127. First, higher volumes of Pluronic (25% w/w) were used to raise the overall concentration. In addition, higher concentrations of NaOH solution were used such that the total amount of NaOH solution would be lower and would not lower the total Pluronic concentration as much. It was found that the higher concentrations of NaOH solutions provided faster diffusion of NaOH through the gels. At the end of synthesis, the samples did not show the

dark color that is indicative of magnetite crystals. This was likely due to the large volume of the overall sample and the lack of a high enough concentration of iron ions.

After this result, attempts were made to use higher concentrations of Pluronic solution initially rather than larger volumes of Pluronic of the same concentration. Thus, 35% and 37% Pluronic F127 solutions (w/w) were used such that the initial concentration of gel was higher than in the previous work. To the gel, the NaOH solution was added. Since the initial gel concentration is much higher, the diffusion of NaOH was much slower and only progressed through a small portion of the gel. Further experiments ensued with lower and lower volumes of 35% or 37% F127 to enable the reaction front to diffuse through a greater percentage of the gel. Eventually, a limit was reached such that using even lower volumes of Pluronic resulted in a liquid suspension rather than a gel at the end of reaction. To deal with this limit, Pluronic was added to the sodium hydroxide solution. By using this approach, even lower volumes of 35% F127 could be used in the initial gel because they would be compensated by the Pluronic in the NaOH solution. Even in this system, the reaction front did not diffuse throughout all the gel. Nevertheless, this system was used as a compromise between having a gel at the end of solution and having adequate diffusion of NaOH. The final concentration of Pluronic F127 in the gel after reaction was 20.4% (w/w), just slightly higher than the experimentally determined cutoff between solution and solid gel, which is 19% (w/w).

The volume of NaOH solution required was calculated based on titration studies. First, solutions containing iron chlorides, buffer, and Pluronic were prepared. Sodium hydroxide

was added to these solutions in increments, and the pH was measured with a pH probe (Microelectrodes, Inc. MI-4146B septa-penetrating probe, Bedford, NH). The pH values with different volumes were recorded and used to create a titration curve (Figure 4.1). For the optimized system, 180μL of 0.5M NaOH (in 13.33% Pluronic F127) was required to raise the pH to 7.6, at which magnetite is formed. In these titration experiments, the formation of magnetite was rapid, as opposed to the longer synthesis experiments, which took two weeks. For the titrations, samples were mixed rapidly by using a Vortex-Genie 2 vortexer (Scientific Industries, Inc., Bohemia, NY). In the optimized system, the solution contents included 320 μL of Pluronic F127 (35% w/w in water), 70 μL of buffer, 50 μL of 0.5M $FeCl_3$, and 50 μL of 0.25M $FeCl_2$.

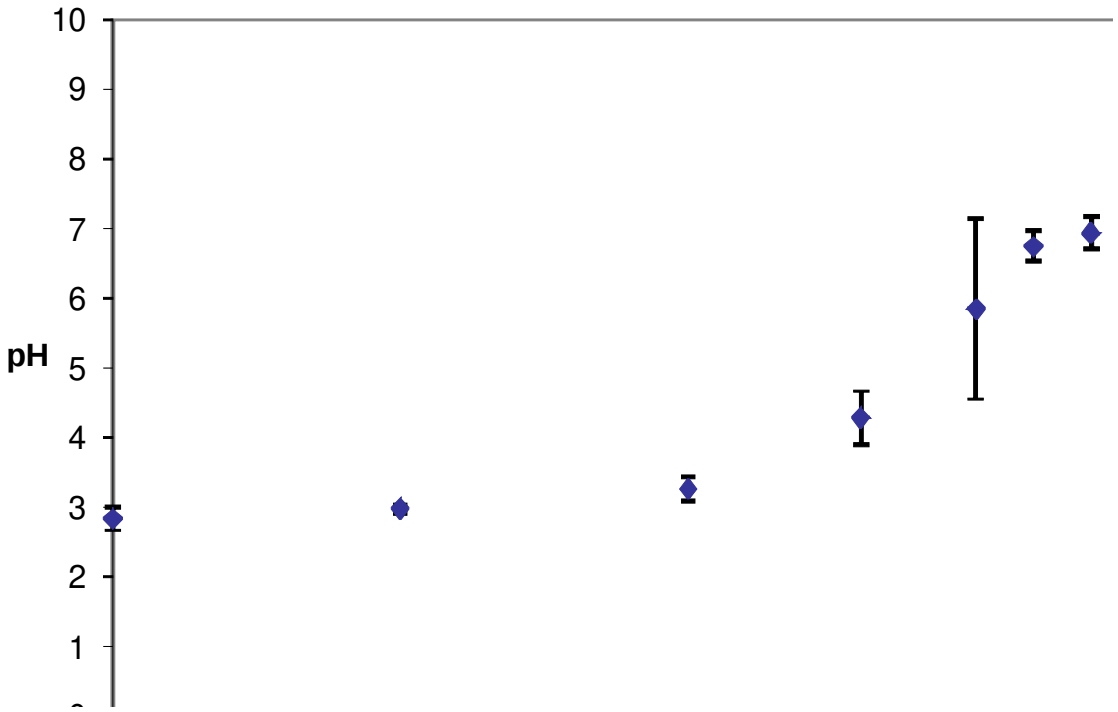

Figure 4.1. Titration curve for magnetite synthesis in solid Pluronic gel. Titrations were completed for three separate samples, so each data point is based on the average of three pH measurements, except for the 160uL condition, for which the pH was measured for only 2 of the samples. Error bars refer to standard deviation.

The preparation of the samples for the longer syntheses was as follows. Protein and buffer were added to 5 mL round or pear-shaped flasks such that their total volume was 70 μL per flask. 320 μL of Pluronic F127 (35%) was added to each flask. The flasks were capped with rubber septa and sealed with cable ties. The flasks were placed over ice or in a refrigerator at 4^{o}C for 30 minutes or longer to provide equilibration of contents. The flasks were degassed and filled repeatedly with argon for about three minutes or longer. This was done through the use of a Schlenk line assembly which had argon and vacuum lines. A needle was inserted into the rubber septa through which the flasks could be degassed and filled with argon. Iron chloride solutions were added (50 μL of 0.5M $FeCl_3$ and 50 μL of 0.25M $FeCl_2$), and the solutions were again degassed and filled with argon in cycles for about 2 minutes or longer. The contents were kept on ice or in a refrigerator at 4^{o}C for 20 minutes or longer to provide equilibration of the iron chlorides with the rest of the contents of the flasks. Afterward, the flasks were kept at room temperature for at least 30 minutes for gelation to occur. To the gel, 180 μL of sodium hydroxide solution (0.5M NaOH in 13.33% Pluronic F127 (w/w)) was added. Over the course of two weeks, the NaOH solution was allowed to diffuse through a portion of the gel and react with the iron chlorides to form magnetite.

Using the optimized system, three concentrations of His-mms6 protein and C25 peptide were studied. In addition, a large number of control samples were prepared for analysis using SAXS, as shown in Table 4.1.

Table 4.1. Control samples for SAXS experiments. For all of the samples, the concentration of Pluronic F127 was 20.4% (w/w) in water.

Pluronic + water
Pluronic + buffer
Pluronic + buffer + His-mms6 (1.5, 20, or 51 ng/μL)
Pluronic + buffer + C25 (0.42, 5.2, or 14 ng/μL)
Pluronic + buffer + $FeCl_2$
Pluronic + buffer + $FeCl_3$
Pluronic + buffer + $FeCl_2$ + $FeCl_3$
Pluronic + buffer + $FeCl_2$ + 14 ng/μL C25
Pluronic + buffer + $FeCl_3$ + 14 ng/μL C25
Pluronic + buffer + $FeCl_2$ + $FeCl_3$ + 14 ng/μL C25
Pluronic + buffer + $FeCl_2$ + 51 ng/μL His-mms6
Pluronic + buffer + $FeCl_3$ + 51 ng/μL His-mms6
Pluronic + buffer + $FeCl_2$ + $FeCl_3$ + His-mms6 (1.5, 20, or 51 ng/μL)
Pluronic + buffer + HCl + NaOH
Pluronic + buffer + HCl + NaOH + 14 ng/μL C25
Pluronic + buffer + HCl + NaOH + 51 ng/μL His-mms6

Sample preparation for SAXS involved the use of Kapton tape and 5mm thick washers (Flat Washer 3.2mm ID x 7.0mm OD x 0.5mm). The sample was placed in the washer and sealed on both sides of the washer with Kapton tape. For air sensitive samples, the samples were prepared inside a nitrogen glove box.

SAXS experiments were conducted at the Advanced Photon Source in Argonne National Laboratory. The 12-ID beam line was used for these experiments. A 168x168 mm square detector (pixel size equal to 164 μm) was used to measure the scattered intensity. A photodiode measured the transmitted intensity of the x-rays, and all data was normalized with it. Samples were held 2m from the detector, and the beam energy used was 12keV. Data was collected at 0.01, 0.1, and 1 s exposures; five exposures were completed per run. The samples containing magnetite scattered very heavily, so 0.01 s exposures were used for analysis. For the other samples, 1 s exposures were adequate. Data was collected over a Q range of 0.01 to 0.28 $Å^{-1}$, where Q is the scattering vector, defined as $Q = 4\pi \sin(\theta/2)/\lambda$, where θ is the scattering angle and λ is the wavelength of the incident X-ray beam [3]. 2D scattering images were obtained, and the 2D data from these images was azimuthally averaged to obtain intensity I versus scattering vector Q data. The absolute intensity was obtained by normalizing with a polyethylene standard as follows:

$$I_{abs\ sam} = \frac{I_{meas\ sam} * I_{abs\ PE,\ Q=0.024\ Å^{-1}} * Thickness_{PE}}{I_{meas\ PE,\ Q=0.024\ Å^{-1}} * Thickness_{sam}}$$

Here, abs= absolute, meas= measured, sam= sample, and PE= polyethylene. The Q value of 0.024 $Å^{-1}$ refers to the first peak position for the PE standard.

4.4. Results

SAXS is a commonly used method for characterizing the structure of condensed matter. SAXS can be used to characterize a number of different samples such as metal alloys, polymers, nanoparticles, and protein solutions [4]. In SAXS, an incident beam of x-rays is directed at the sample, and scattered x-rays hit a detector at small angles of less than one degree relative to the incident beam [3, 5, 6]. The intensities of these x-rays are recorded along with the scattering angles [4, 7].

SAXS data is presented as absolute scattering intensity versus Q, where Q is the scattering vector, the inverse of which is related to characteristic length scales in the sample [3]. Particularly, the first peak position, referred to as Q*, is an indicator of the inter-micellar distance in the Pluronic medium [8]. The peak positions to the right of the first peak are an indicator of the FCC structure of the system. A perfect FCC structure has Q/Q* ratios of $\sqrt{3}:\sqrt{4}:\sqrt{8}:\sqrt{11}:\sqrt{12}$. The closer the ratios of the experimental sample to the theoretical FCC ratios, the greater the extent of the FCC structure in the sample [8]. Figure 4.2 is a representative SAXS plot for Pluronic F127 alone (20.4% w/w). For a perfect FCC structure, there should be at least five distinct peaks. The Pluronic sample exhibits four peaks, as shown in Figure 4.2. All four of these peaks fit the FCC theoretical ratios very well, indicating that the Pluronic alone has a close to perfect FCC structure. Figure 4.3 shows the SAXS data for Pluronic after buffer is added to it. It is clear that the buffer does not perturb the FCC structure of the Pluronic since the Q/Q* experimental ratios are close to that of an FCC structure.

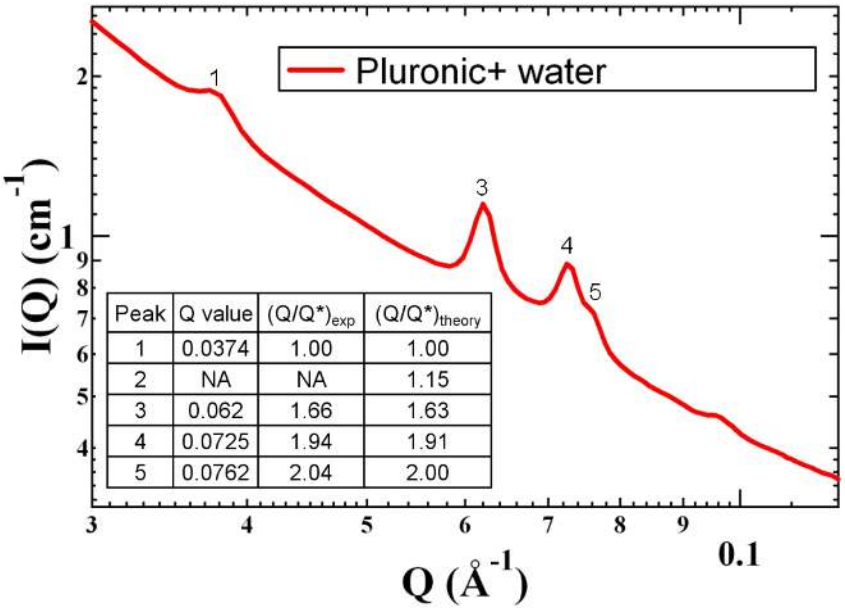

Figure 4.2. SAXS plot for Pluronic F127 in water (20.4% w/w). The table in the inset gives Q/Q* values for the experimental Pluronic sample and compares them to the perfect, theoretical FCC structure ratios. Peak positions are labeled in the figure. The designation "NA" indicates that the peak was not clearly apparent.

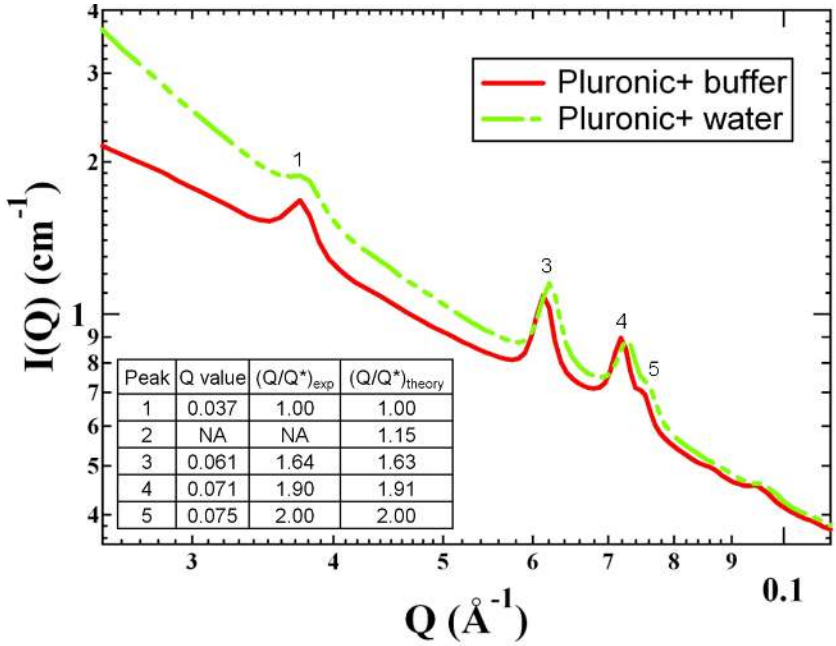

Figure 4.3. SAXS plot for Pluronic F127 (20.4% w/w) and buffer in water. Peak positions are labeled as shown. The Pluronic + water sample is shown as a reference. The designation "NA" indicates that the peak was not clearly apparent.

Figure 4.4 shows the SAXS data for the control experiment when C25 protein is added to the Pluronic and buffer. The data shows that the Q/Q* values fit the FCC values for 4 of the 5 peaks, regardless of the concentration of protein. This indicates that the C25 protein does not perturb the FCC structure of the Pluronic. Also, the peaks line up well with the ones from the Pluronic, indicating that the micellar structure of the Pluronic remains intact. Figure 4.5 shows the SAXS data for the case when His-mms6 is added to the Pluronic and buffer. In this case, the Q/Q* ratios are perturbed slightly but not significantly, as noted from their departure from the characteristic ratios for the FCC structure for the highest His-mms6 concentration. This indicates that at high concentrations, His-mms6 slightly perturbs the Pluronic's FCC structure. This result is not surprising because His-mms6 is a bigger protein than C25.

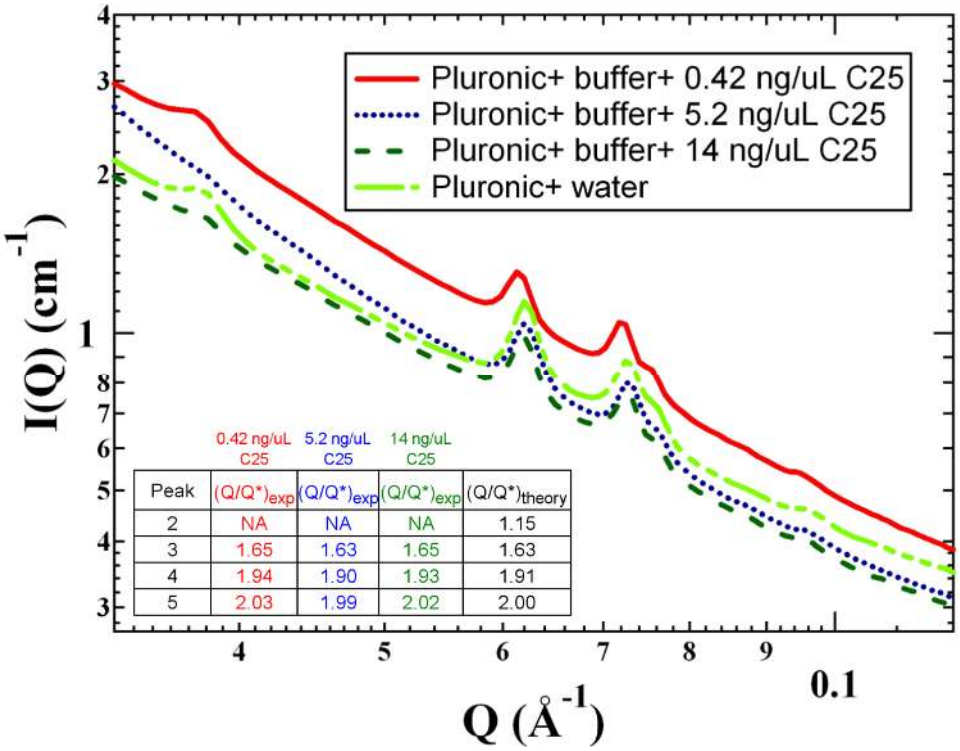

Figure 4.4. SAXS plot for Pluronic F127 (20.4% w/w), buffer, and three different concentrations of C25 in water The Pluronic + water sample is shown as a reference. The designation "NA" indicates that the peak was not clearly apparent.

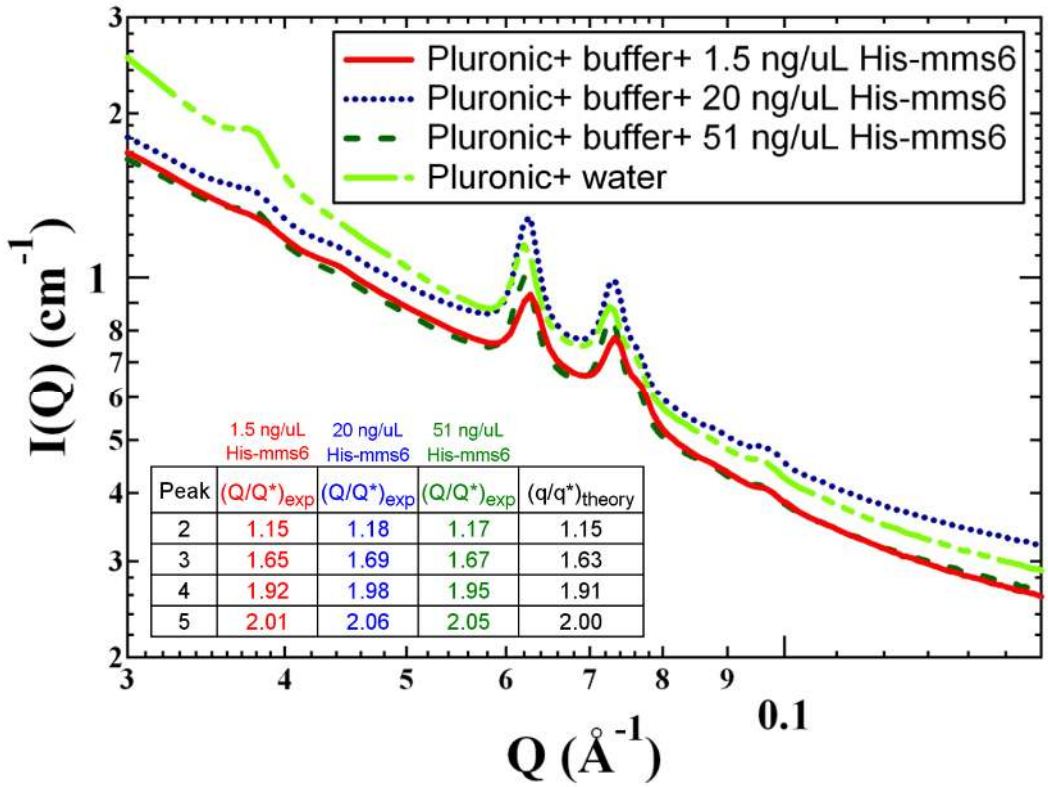

Figure 4.5. SAXS plot for Pluronic F127 (20.4% w/w), buffer, and three different concentrations of His-mms6. The Pluronic + water sample is shown as a reference.

Figure 4.6 shows the SAXS data for the control experiment when NaOH and HCl react in the presence of Pluronic and buffer, forming NaCl crystals. Note that the Q/Q* values fit the FCC values for all of the five peaks, regardless of the presence or absence of either the C25 or His-mms6 protein. Also, four of the peaks line up well with the four peaks from the Pluronic, indicating that the micellar structure of the Pluronic remains intact. The fifth peak for the NaCl samples indicates that the micellar structure of the Pluronic in the presence of salt has more well-defined FCC characteristics. These experiments indicate that the NaCl crystals do not disrupt the FCC structure of the Pluronic.

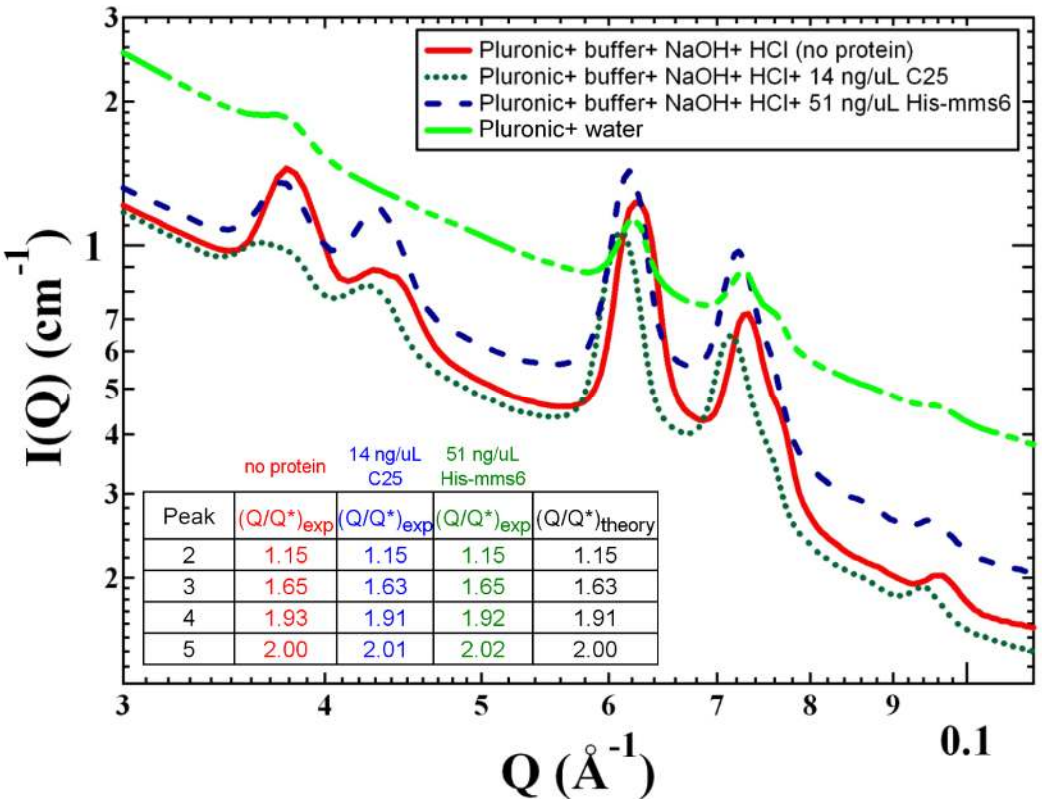

Figure 4.6. SAXS plot for Pluronic F127 (20.4% w/w), buffer, NaOH, HCl, and proteins in water. The Pluronic + water sample is shown as a reference.

Figure 4.7 shows the SAXS data for the control experiment when iron chlorides are added to the Pluronic and buffer. It is observed that for the case of addition of $FeCl_3$ the Q/Q* ratios for all five peaks line up with the FCC structure ratios. This is also the case for the addition of both $FeCl_2$ and $FeCl_3$. The addition of mixed chlorides may stabilize the Pluronic structure due to electrostatic interactions, leading to enhancement of the FCC structure. However, for the addition of $FeCl_2$ alone, the Q* peak does not exist, indicating a perturbed Pluronic structure. Figure 4.8 shows the case when iron chlorides are added along with the highest concentration of C25 protein to the Pluronic and buffer. In this case, the addition of $FeCl_3$ alone perturbs the Pluronic structure, but for the other two cases the FCC structure is maintained based on the Q/Q* ratios.

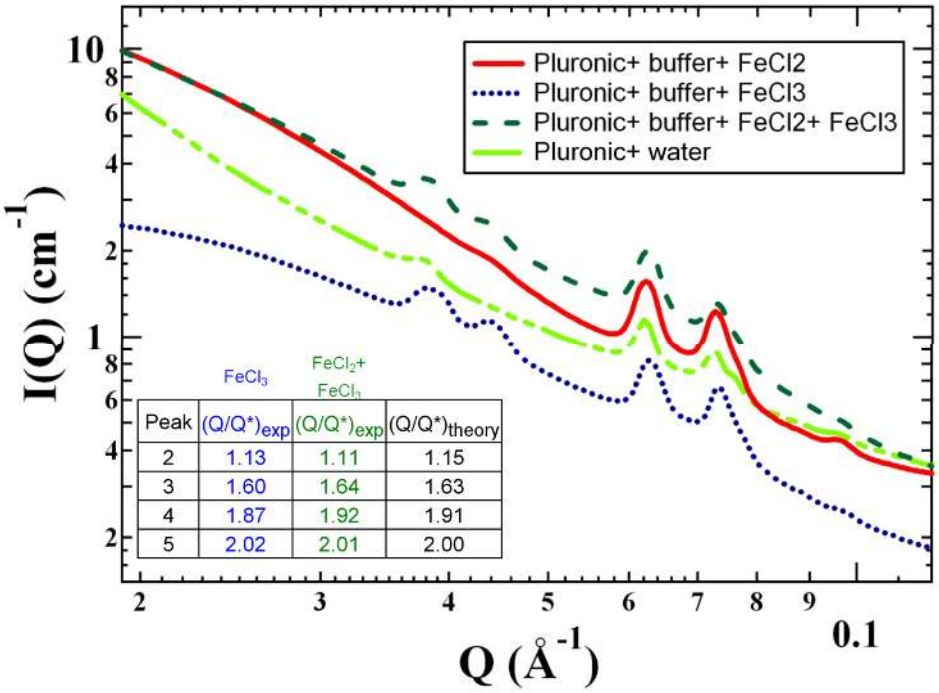

Figure 4.7. SAXS plot for Pluronic F127 (20.4% w/w), buffer, and iron chlorides in water. The Pluronic + water sample is shown as a reference. Note that the $FeCl_2$ sample lacked a clear Q* peak, so FCC peak analysis could not be completed.

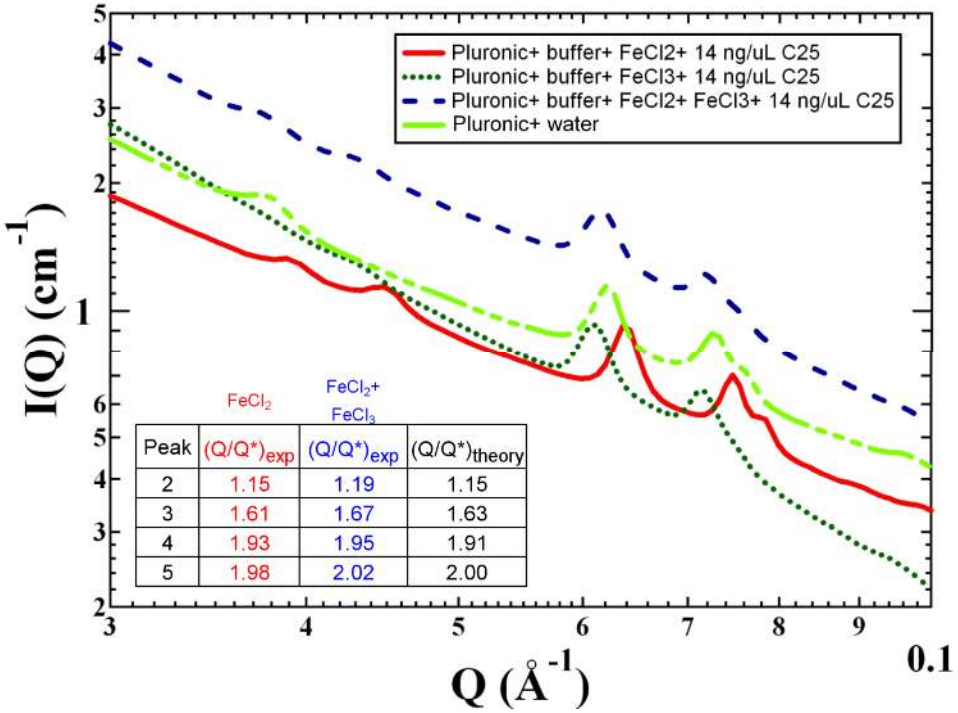

Figure 4.8. SAXS plot for Pluronic F127 (20.4% w/w), buffer, iron chlorides, and C25 in water. The Pluronic + water sample is shown as a reference. Note that the $FeCl_3$ sample lacked a clear Q* peak, so FCC peak analysis could not be completed.

For the case of the addition of the highest concentration of His-mms6 and iron chlorides, Figure 4.9 shows that when $FeCl_2$ and $FeCl_3$ are added individually, the Pluronic structure matches the FCC structure ratios very well. However, when both iron chlorides are added, the Q* peak is missing, indicating that the FCC structure of the Pluronic is perturbed. Figure 4.10 shows the case when both iron chlorides are added and the His-mms6 protein concentration is varied. For the low and intermediate concentrations of His-mms6, the Pluronic FCC structure is preserved, but for the highest concentration of His-mms6, the Q* peak is missing, indicating a Pluronic structure that is perturbed from the FCC structure.

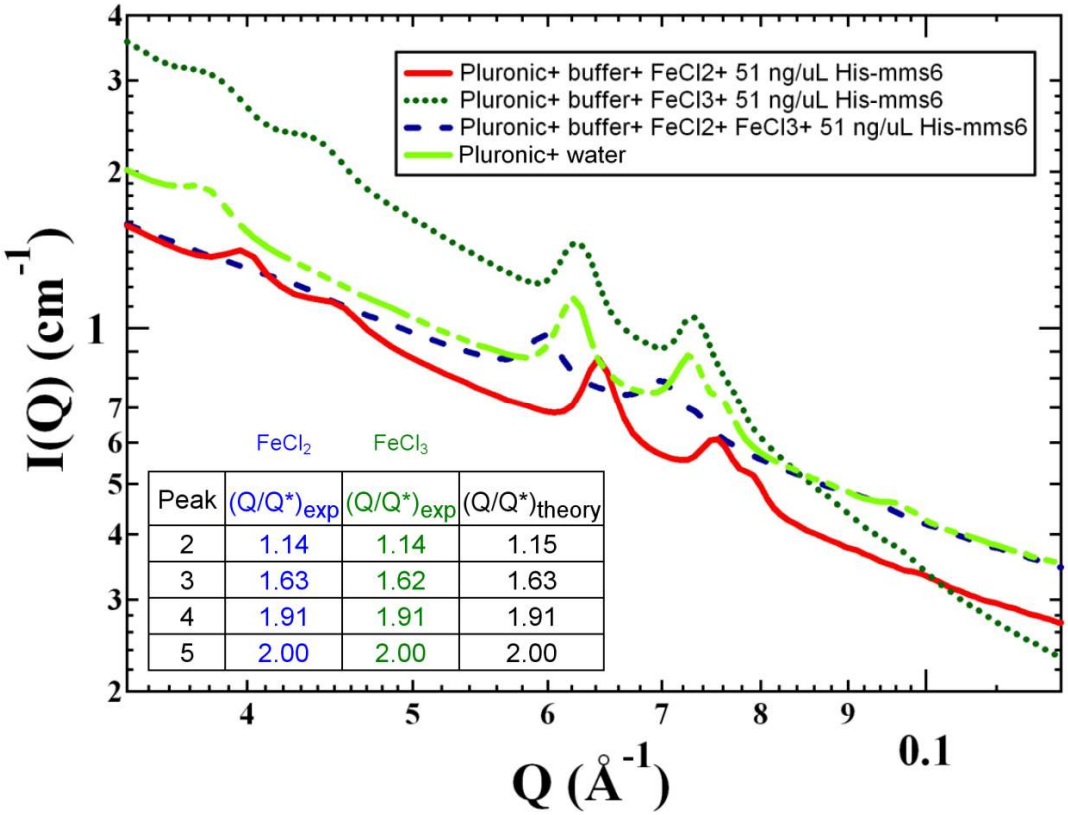

Figure 4.9. SAXS plot for Pluronic F127 (20.4% w/w), buffer, iron chlorides, and His-mms6 in water. The Pluronic + water sample is shown as a reference. Note that the $FeCl_2$+$FeCl_3$ sample lacked a clear Q* peak, so FCC peak analysis could not be completed.

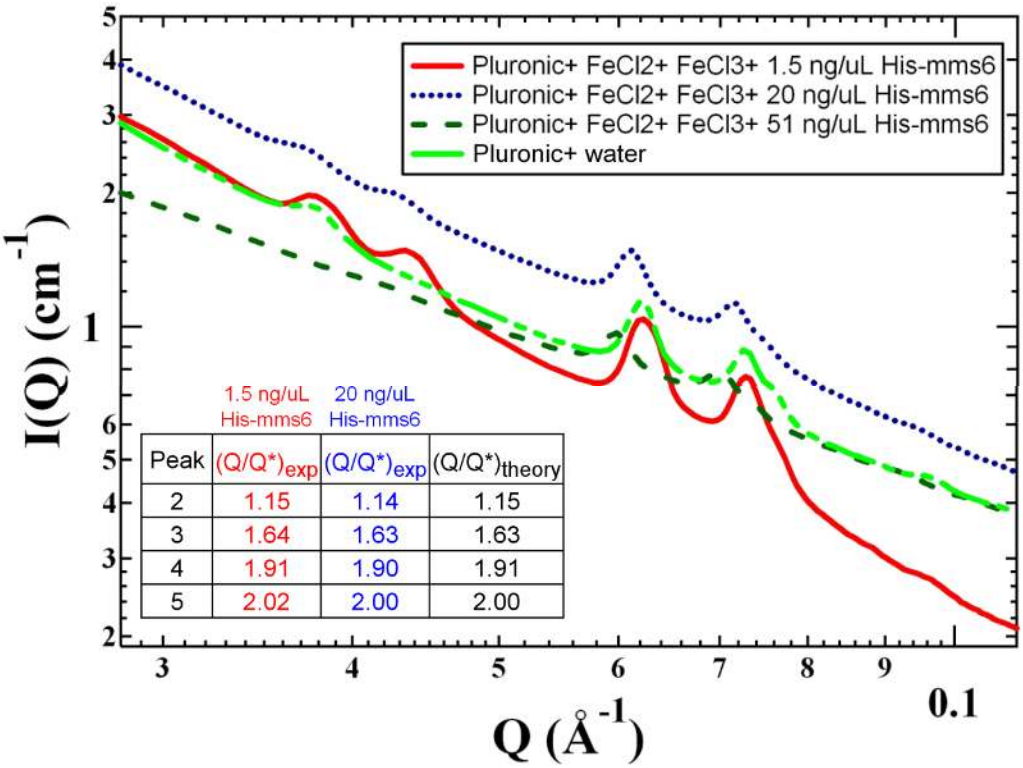

Peak	(Q/Q*)exp 1.5 ng/uL His-mms6	(Q/Q*)exp 20 ng/uL His-mms6	(Q/Q*)theory
2	1.15	1.14	1.15
3	1.64	1.63	1.63
4	1.91	1.90	1.91
5	2.02	2.00	2.00

Figure 4.10. SAXS plot for Pluronic F127 (20.4% w/w), buffer, both iron chlorides, and varying concentrations of His-mms6 in water. The Pluronic + water sample is shown as a reference. Note that the sample with the highest concentration of His-mms6 lacked a clear Q* peak, so FCC peak analysis could not be completed.

Figure 4.11 shows the data for the experiment in which magnetite is in the Pluronic medium along with buffer in the presence of varying concentrations of C25. Note that the intensity of these samples is much greater than that of the other samples in the SAXS plots previously shown due to the strong electron density gradient because of the magnetite. In Figure 4.11, the Pluronic curve is shifted vertically upward for ease of comparison, however the intensity of the Pluronic curve is about two orders of magnitude lower than that of the magnetite curves. The heavy scattering from the magnetite particles makes it difficult to identify all the Pluronic peaks. Some peaks, however, can be identified, including the first Q* peak. Based on the peaks that can be identified, the ratios line up with the FCC structure, but many peaks

are missing, indicating either that there is some perturbation of the FCC structure or that it is not possible to see these peaks due to the strong scattering of the magnetic particles. The peaks that do exist are not thought to be from the magnetite particles themselves because the particles have a very broad size distribution and would not give characteristic peaks. Rather, the presence of particles would shift the curves upward and cause the Pluronic structure to change.

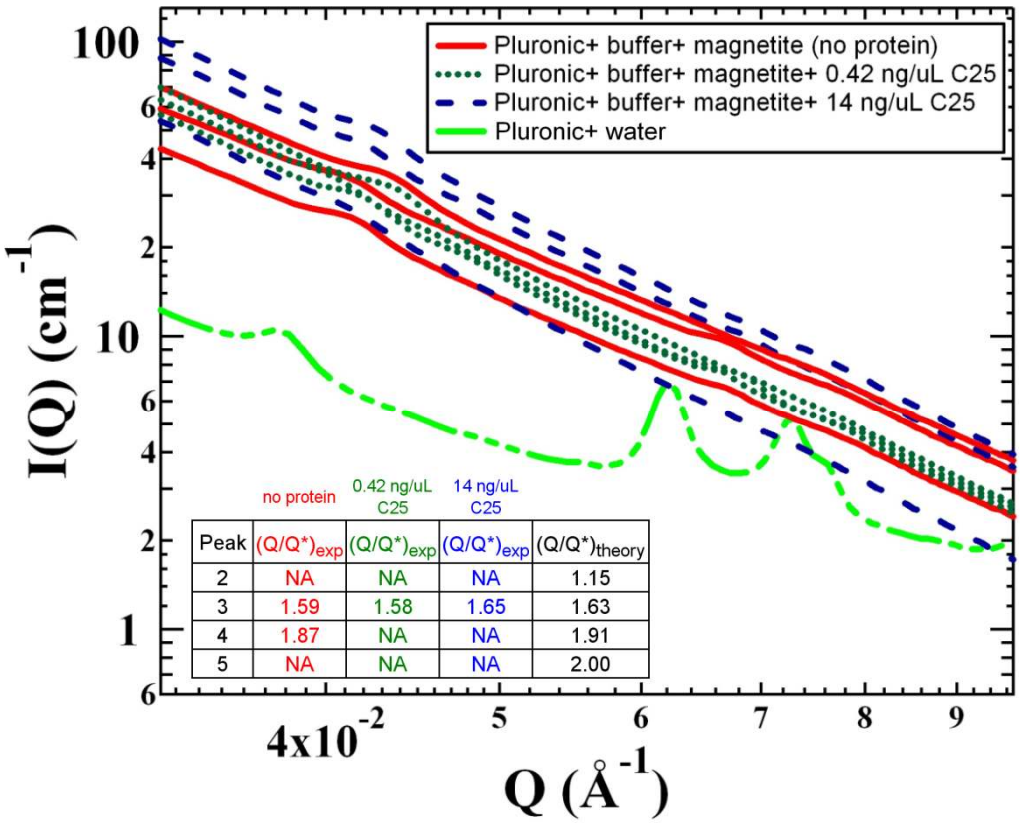

Peak	$(Q/Q^*)_{exp}$ no protein	$(Q/Q^*)_{exp}$ 0.42 ng/uL C25	$(Q/Q^*)_{exp}$ 14 ng/uL C25	$(Q/Q^*)_{theory}$
2	NA	NA	NA	1.15
3	1.59	1.58	1.65	1.63
4	1.87	NA	NA	1.91
5	NA	NA	NA	2.00

Figure 4.11. SAXS plot for Pluronic F127 (20.4% w/w), buffer, magnetite, and varying concentrations of C25 in water. The Pluronic + water sample is shown as a reference.

Figure 4.12 shows the SAXS data when magnetite particles are embedded in Pluronic gel in the presence of buffer at varying concentrations of His-mms6. It is observed that for the lowest concentration of His-mms6, the Q/Q* ratios are reasonably close to the FCC ratios,

for the peaks that can be identified. However, as the His-mms6 protein concentration is increased, the Q/Q* ratios deviate more and more from the FCC ratios, indicating that the magnetite in the presence of higher His-mms6 protein concentrations is perturbing the Pluronic structure to a larger extent.

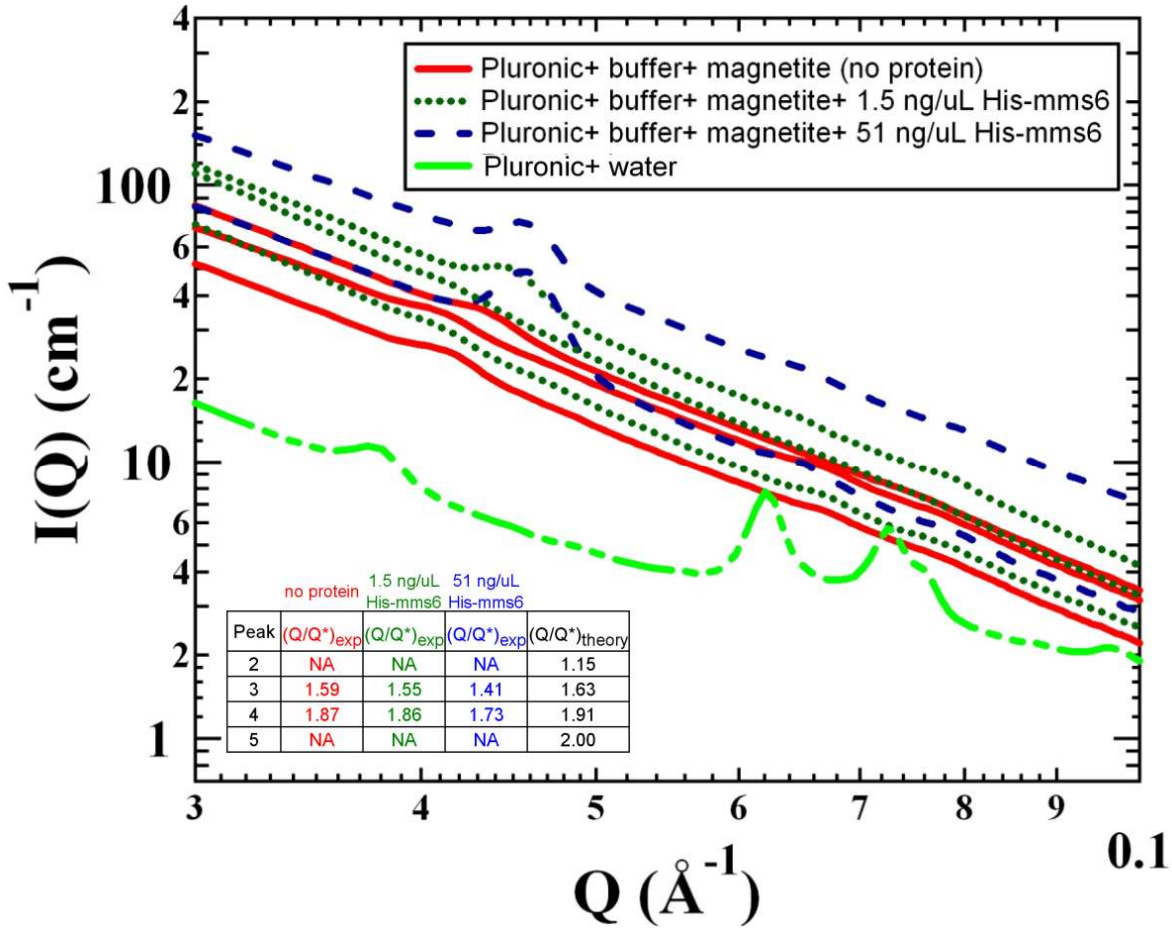

Peak	no protein $(Q/Q^*)_{exp}$	1.5 ng/uL His-mms6 $(Q/Q^*)_{exp}$	51 ng/uL His-mms6 $(Q/Q^*)_{exp}$	$(Q/Q^*)_{theory}$
2	NA	NA	NA	1.15
3	1.59	1.55	1.41	1.63
4	1.87	1.86	1.73	1.91
5	NA	NA	NA	2.00

Figure 4.12. SAXS plot for Pluronic F127 (20.4% w/w), buffer, magnetite, and varying concentrations of His-mms6 in water. The Pluronic + water sample is shown as a reference.

As mentioned before, the first peak position Q* is an indicator of the inter-micellar distance. This distance, D, is calculated as follows [8]:

$$D=\sqrt{3}d_{111} \text{ where } d_{111}=\frac{2\pi}{Q^*}$$

Therefore, from the Q value of the first peak position in the magnetite curves, Q*, the Pluronic inter-micellar distance can be calculated. Table 4.2 shows how the inter-micellar distance changes with C25 protein concentration. The data indicate that there is no characteristic trend in the inter-micellar distance with C25 concentration. Table 4.3 shows how the inter-micellar distance changes with His-mms6 concentration. For no protein and a low concentration of His-mms6, the inter-micellar distance is almost the same. However, as the concentration of His-mms6 increases, the distance decreases. The statistical significance of the highest His-mms6 concentration case is evident when compared to the no-protein case using an unpaired student's t-test ($p<0.05$) but is not evident when comparing to the low concentration case ($p>0.1$).

Table 4.2. Effect of C25 protein concentration on characteristic inter-micellar distance. Data presented as mean ± s. d.

Concentration of C25 (ng/uL)	Characteristic Distance D (nm)
0	26.0 ± 0.8
0.42	25.7 ± 1.3
14	26.1 ± 0.5

Table 4.3. Effect of His-mms6 protein concentration on characteristic inter-micellar distance. Data presented as mean ± s. d.

Concentration of His-mms6 (ng/uL)	Characteristic Distance D (nm)
0	26.0 ± 0.8
1.5	25.9 ± 1.4
51	24.2 ± 0.8

Transmission electron microscopy (TEM) studies were performed by Dr. Tanya Prozorov to complement the SAXS results. Figure 4.13 shows TEM images for the case of magnetite synthesis with no protein. The particles are highly polydisperse, with sizes ranging from less than 5 nm to 17 nm. For the case of magnetite synthesis with 0.42 ng/μL C25 (Figure 4.14),

the particles are polydisperse. Most of the particles are less than 10 nm, although there are particles as large as 15 nm. The same is the case for particles synthesized in the presence of 14 ng/μL C25 (Figure 4.15).

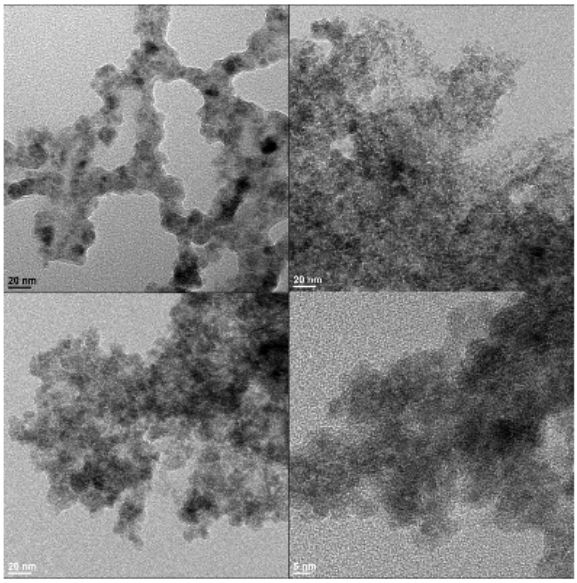

Figure 4.13. Selected TEM images of magnetite synthesized in the presence of no protein. Scale bars are all 20nm, except for the lower right image (5 nm).

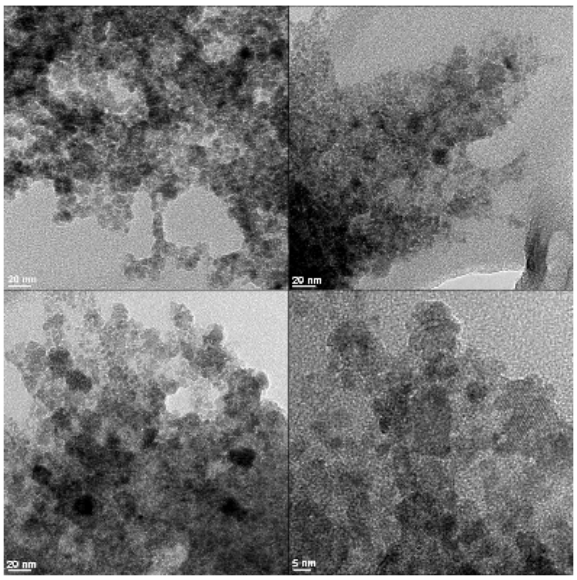

Figure 4.14. Selected TEM images of magnetite synthesized in the presence of 0.42 ng/μL C25. Scale bars are all 20nm, except for the lower right image (5 nm).

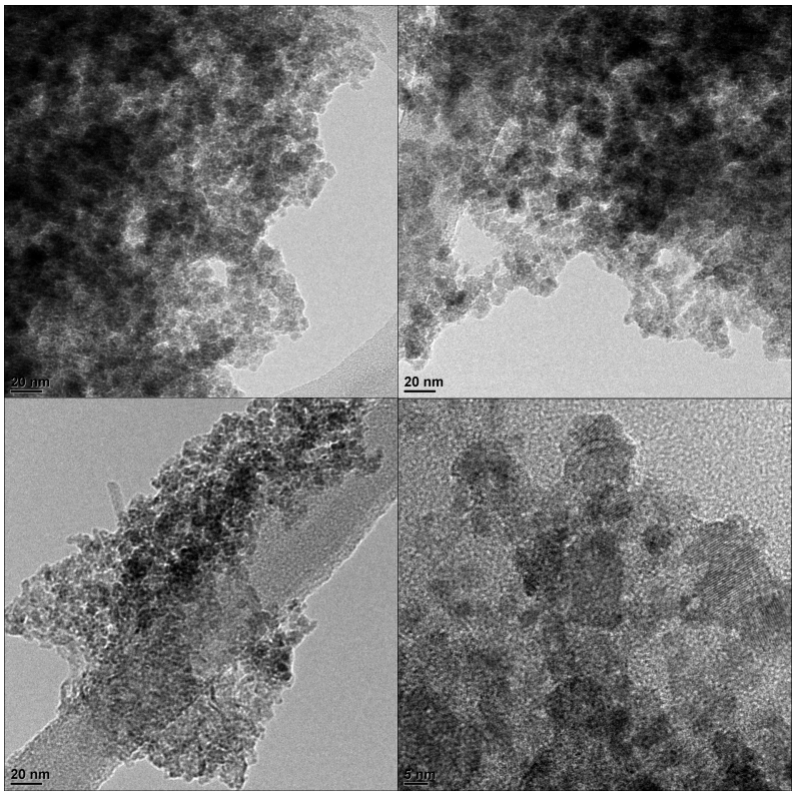

Figure 4.15. Selected TEM images of magnetite synthesized in the presence of 14 ng/μL C25. Scale bars are all 20nm, except for the lower right image (5 nm).

In the presence of 1.5 ng/μL His-mms6, there appear to be more well defined particles, as shown in Figure 4.16, although the particles are still polydisperse. There are many particles less than 10 nm in size, but there are particles as large as 20 nm. Figure 4.17 shows magnetite particles synthesized in the presence of 51 ng/μL His-mms6; the particles are polydisperse but appear less well defined, and the particle sizes are smaller, with particles only as large as 11 nm.

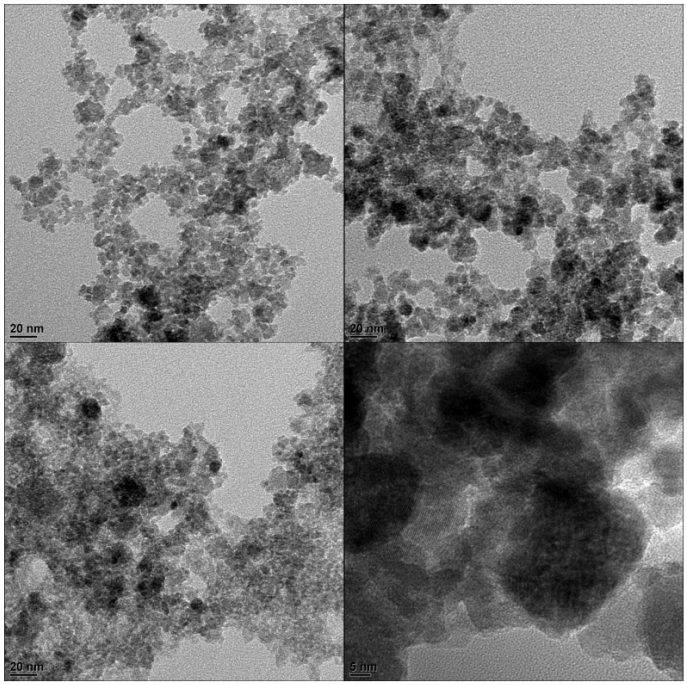

Figure 4.16. Selected TEM images of magnetite synthesized in the presence of 1.5 ng/μL His-mms6. Scale bars are all 20 nm, except for the lower right image (5 nm).

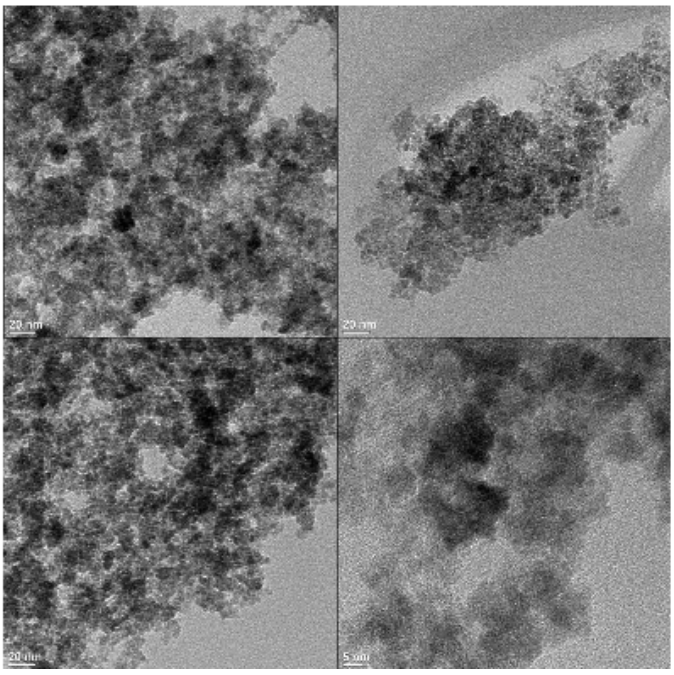

Figure 4.17. Selected TEM images of magnetite synthesized in the presence of 51 ng/μL His-mms6. Scale bars are all 20 nm, except for the lower right image (5 nm).

4.5. Discussion

It is thought that an FCC structure, given its ordered packing, will enhance the magnetite templating ability of both the C25 and His-mms6 proteins. In this study, it has been shown that the FCC structure of the Pluronic is maintained in the presence of either protein. In the presence of both iron chlorides, the FCC structure is maintained and even enhanced. Due to the charged nature of both the Pluronic and iron chlorides, it is possible that the iron chlorides together enhance the self-assembly and consequently the FCC structure of the Pluronic due to charge stabilization. When iron chlorides are used along with either protein, some combinations disrupt the FCC structure, while others preserve the structure. In the presence of magnetite particles, it appears that either the FCC structure is disrupted or that the high level of scattering from the particles "shields" the effect of the Pluronic. In the SAXS data for the experiments with magnetite, it does appear that the scattering from the particles shields most of the effect of the Pluronic structure. However, there is still evidence of residual peaks that are likely attributable to the Pluronic structure.

The evidence that these peaks belong to the Pluronic is two-fold. First, there is a distinct first peak in every magnetite curve that is characteristic of the Pluronic. It is shifted horizontally to the right somewhat, but it has the same characteristic shape as that of the first peak for the Pluronic sample, as shown in Figures 4.11 and 4.12. It is possible that the shift is due to the Pluronic structure being compressed because of the magnetic particles that are in their vicinity. As the particles grow, it is reasonable to expect them to compress the Pluronic micelles around them as there is less space available for the micelles (Figure 4.18).

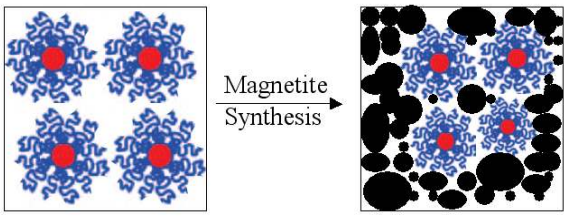

Figure 4.18. A possible scenario of the compression of the Pluronic micelles due to spatial limitations in the presence of magnetite. Figure modified from [2].

Second, the ratios of the higher order peaks to the first peak (Q/Q*) match the theoretical FCC ratios rather well for the case of C25 templating. For the case of His-mms6, the Q/Q* ratios are close to the FCC ratios for the lowest His-mms6 concentration, but as the protein concentration increases, the deviation of the ratios from the FCC ratios grows. This is to be expected for His-mms6 as opposed to C25 because His-mms6 is a larger protein. Since the magnetite is presumably bound to the His-mms6, as the magnetite grows, these magnetite-His-mms6 complexes would compress and eventually disrupt the FCC structure of the Pluronic (Figure 4.19). This is not the case for magnetite-C25 complexes possibly because the C25 is smaller and would therefore not compress the Pluronic as much (Figure 4.20).

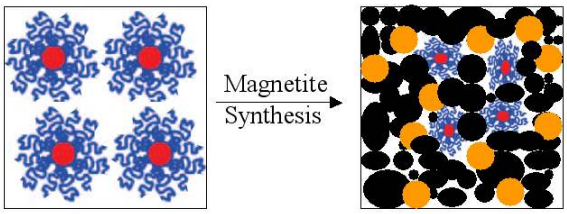

Figure 4.19. A possible scenario of the compression and disruption of the Pluronic micelles due to spatial limitations in the presence of magnetite and the His-mms6 protein. Figure modified from [10].

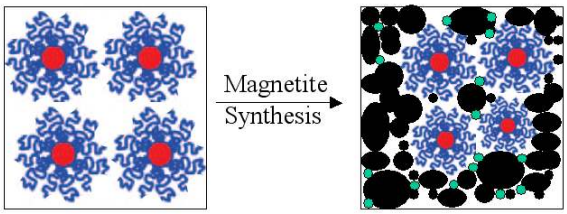

Figure 4.20. A possible scenario of the compression (but not disruption) of the Pluronic micelles due to spatial limitations in the presence of magnetite and the C25 protein. Figure modified from [2].

As the C25 protein concentration increases, there appears to be no effect on inter-micellar distance. For low concentrations of His-mms6, there appears to be no difference in inter-micellar distance when compared to the "no protein" case. However, as indicated in Table 4.3, the inter-micellar distance decreases with increase in the His-mms6 concentration. As the FCC structure is compressed and disrupted, it is reasonable to expect a smaller inter-micellar distance as the micelles become disorganized and begin to re-arrange themselves closer to each other.

From the TEM studies, the particles synthesized in the presence or absence of C25 or His-mms6 are polydisperse. There are regions in the samples that contain larger particles and regions containing smaller particles for both C25 concentrations and the lower concentration of His-mms6. For the higher concentration of His-mms6, there was a lack of large particles, which may be due to the disruption of the Pluronic F127 gel as evidenced by the FCC ratio calculations from the SAXS data. For the case of magnetite synthesis without protein, there are not only small particles but also large, well-defined particles. This is a surprising result because it is thought that the C25 and His-mms6 proteins are needed for the synthesis of large magnetite particles. This result indicates that the protein is not necessarily needed for

the formation of large, fairly uniform magnetite particles in the solid Pluronic gel system. This may suggest that the Pluronic gel itself may be templating particle formation. Indeed, for the case of the higher His-mms6 concentration, disruption of the FCC structure of the Pluronic gel coincided with smaller particle sizes. This may suggest that the Pluronic gel with an FCC structure is able to template magnetite particle formation without protein. This is in contrast to the solution phase studies, for which the Pluronic solution did not have an FCC structure because it was not a solid gel and where the His-mms6 (or C25) protein was necessary for the synthesis of large, uniform magnetite particles.

The TEM studies show the presence of small and large particles in the presence and absence of C25 and His-mms6 proteins. Overall, the particle sizes are smaller than those synthesized in the solution phase experiments (~30 nm) [1]. This cannot be fully explained by disruption of FCC structure in the Pluronic gel when magnetite is synthesized. The SAXS data indicates that the magnetite samples preserve at least some peaks that correspond to the FCC structure in the presence of C25, no protein, and a low concentration of His-mms6. Rather, the viscosity of the Pluronic gel medium is likely to have a more significant effect on the magnetite particle size. In the previous studies, magnetite synthesis was carried out in solution phase, so diffusion of reagents occurred much more readily. In our experiments, due to the higher viscosity of the Pluronic solid gel, diffusion limitations lead to the formation of smaller particles. Indeed, the viscosity of Pluronic F127 gel at 25% (w/w) is two orders of magnitude higher than the viscosity for solution phase experiments, for which the Pluronic concentration was about 12% (w/w) [9, 10]. Another reason for the smaller particles may be

the compression of the particles due to the Pluronic micelles in solid state, which may impede growth of particles.

4.6. Conclusions

This study has shown that the proteins alone do not affect the Pluronic structure, except slightly for the case of the highest concentration of His-mms6. In addition, mixed chlorides may act to stabilize the self-organization of the Pluronic due in electrostatic interactions. This study has shown that magnetite synthesis in Pluronic is a function of several parameters including the concentration and size of the protein used for templating, the concentration of the magnetite, and the viscosity of the Pluronic gel. Our results indicate that magnetite particle synthesis in Pluronic causes the inter-micellar distance to decrease, most notably for the case of the highest concentration of His-mms6. This may be attributed to an apparent compression in the gel because of the magnetite particles and the large size of His-mms6. Large magnetite particles can be formed in solid Pluronic gel in the absence of protein, indicating that Pluronic alone may template particle synthesis. This is in contrast to magnetite formation in the solution phase, for which either the His-mms6 or C25 protein is required for templating. Disruption in the FCC structure is observed for the case of the highest His-mms6 concentration, which is consistent with the larger size of the His-mms6 protein. Disruption of the FCC structure may eliminate the possible templating ability of the Pluronic gel, as evidenced by the lack of large particles present in the case of the highest His-mms6 concentration. The large scattering due to the magnetite particles suggests the use of a lower concentration of iron chlorides so as to be able to resolve all the higher order peaks in the gel. Compared to the solution phase experiments, the solid gel phase synthesis method results in a

gel with a much higher viscosity, which is likely to impede particle growth. Thus, the viscosity of the gel may be used to control the particle size in the biomineralization synthesis platform.

4.7. References

1. Prozorov, T.; Mallapragada, S. K.; Narasimhan, B.; Wang, L.; Palo, P.; Nilsen-Hamilton, M.; Williams, T. J.; Bazylinski, D. A.; Prozorov, R.; Canfield, P. C. Protein-Mediated Synthesis of Uniform Superparamagnetic Magnetite Nanocrystals. *Adv. Funct. Mater.* **2007**, *17*, 951–957.

2. Prozorov, T.; Palo, P.; Wang, L.; Nilsen-Hamilton, M.; Jones, D.; Orr, D.; Mallapragada, S.K.; Narasimhan, B.; Canfield, P.C.; Prozorov, R. Cobalt ferrite nanocrystals: outperforming magnetotactic bacteria. *ACS Nano*. **2007**, 1, 228–233.

3. Roe, R. Methods of X-Ray and Neutron Scattering in Polymer Science. Oxford University Press. **2000**, pp. 8, 155.

4. Saxier (European Molecular Biology Laboratory). What is Synchroton SAXS? : Small-Angle X-ray Scattering Explained. http://www.saxier.org/ aboutus/saxs.shtml (accessed May 6, 2008).

5. Singh, M. A Brief Overview of SAXS. Queen's University Physics Department. http://www.physics.queensu.ca/~saxs/ SAXSoverview.html (accessed August 21, 2008).

6. Vachette, P.; Svergun, D.I. Small-angle X-ray scattering by solutions of biological macromolecules. In "Structure and Dynamics of Biomolecules." Fanchon, E.; Geissler, G.; Hodeau , J.-L.; Regnard, J.-R.; Timmins, P.A. (eds.). New York: Oxford University Press. **2000**, 199-237.

7. Geerlof, A.; Brown, J.; Coutard, B.; Egloff, M. P.; Enguita, F. J.; Fogg, M. J.; Gilbert, R. J. C.; Groves, M. R.; Haouz, A.; Nettleship, J. E.; Nordlund, P.; Owens, R. J.; Ruff, M.; Sainsbury, S.; Svergun, D. I.; Wilmanns, M. The impact of protein characterization in structural proteomics. *Acta Cryst*. **2006**, D62, 1125–1136.

8. Enlow, D.; Rawal, A.; Kanapathipillai, M.; Schmidt-Rohr, K.; Mallapragada, S.; Lo, C. T.; Thiyagarajan, P.; Akinc, M. Synthesis and characterization of self-assembled block copolymer templated calcium phosphate nanocomposite gels. *J. Mater. Chem*. **2007**, 17, 1570-1578.

9. Maheshwari, M.; Miglani, G.; Mali, A.; Paradkar, A.; Yamamura, S.; Kadam, S. Development of tetracycline - serratiopeptidase - containing periodontal gel: formulation and preliminary clinical study. *AAPS PharmSciTech.* **2006**, 7(3), 76.

10. Trong, L. C. P.; Djabourov, M.; Ponton, A. Mechanisms of micellization and rheology of PEO-PPO-PEO triblock copolymers with various architectures. *Journal of Colloid and Interface Science*. **2008**, 328 (2), 278-287.

CHAPTER 5. FUTURE WORK

5.1. Future Work

Future work can be focused on the development of a system in which viscosity limitations are overcome. Although the viscosity can in principle be lowered by using a more dilute Pluronic, this is problematic because if the Pluronic is diluted there may not be a solid gel during synthesis. In the current study, the final concentration of the gel is about 20.4% (w/w) in water, while the cutoff between a gel and a solution is about 19% (w/w) in water. Therefore, there is not room for improvement in this regard. However, future work could include the use of other Pluronics that have lower molecular weights than Pluronic F127. The lower viscosities of these systems could enable the formation of larger magnetite particles in the gel phase. Also, if it is true that an FCC structure does enhance particle formation for less viscous systems, Pluronics should be sought that have a native FCC structure, and SAXS experiments may be conducted using these systems.

In addition to system optimization and SAXS studies, future work can also include studies involving magnetite synthesis on a flat surface in the presence of His-mms6 and C25 proteins attached to that surface. In particular, protein in buffer solution can be placed into a well. The bottom of the well could be hydrophobic such that the hydrophobic terminal region of the protein will adsorb to this surface (e.g., gold). Depending on the conformation of the protein, the hydrophilic terminal region may or may not be exposed. Cold aqueous Pluronic F127

solution can be added on top of the adsorbed protein. Afterward, iron chloride solutions can be added. The well plate can be kept over ice to allow proper mixing. The well plate can be taken off the ice and heated to 37^{o}C so that the solution forms a gel. Sodium hydroxide can then be added on top of the gel, where it should slowly diffuse into the gel. Ideally, magnetite crystals will nucleate on the protein and remain attached to the protein (Figure 5.1).

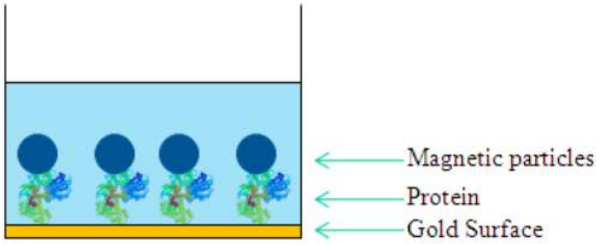

Figure 5.1. Schematic of proposed protein templating in a well [1].

When the magnetite is formed, most of it will be synthesized without protein templating as the sodium hydroxide diffuses through the gel. Only the magnetite formed at the very bottom of the gel in contact with the protein will have protein templating. The sample can be placed on ice to make the gel turn to liquid, and the liquid can be washed off; the liquid will contain magnetite not formed in the presence of protein. The magnetite formed using protein templating will presumably be bound to the protein at the surface and thus will not be washed away. A magnet can be placed on the other side of the well, and a wash solution for which the protein has a high affinity can be used to wash away the protein, leaving behind the magnetite particles. The magnet can then be removed, and the magnetite particles will be allowed to go into aqueous solution above it. A portion of this aqueous solution can be used for analysis, most notably TEM. Since TEM requires very dilute concentrations of solute for clear visualization of individual particles, the low concentration of magnetite particles that have been templated with protein in the well will be suitable. These studies can help

understand how the protein conformation may template particle synthesis. If it is observed that particles do nucleate and grow on the protein, this could indicate the presence of hydrophilic groups sticking up freely from the surface. On the other hand, if particles do not nucleate on the surface, this may indicate that the hydrophilic groups of the protein are not freely exposed or that there is some steric hindrance when the hydrophobic parts are attached to the well surface.

Synthesis of new types of magnetic particles may also be pursued. Synthesis of new types of magnetic particles is advantageous for a number of reasons. One is that new particles may have better magnetic properties than either magnetite or cobalt ferrite. Another is that their possible synthesis using the mms6 protein and the short C25 version could give further clues as to the conformation and templating mechanism of the proteins. MFe_2O_4 particle synthesis (where M= Fe, Co, Mn, Ho, Gd, etc.) has already been started by our group (for M= Fe and Co) with favorable results when using the mms6 protein and its shorter peptide version, indicating that synthesis of more of these types of particles is worthwhile exploring [2, 3]. Synthesis of other types of magnetic particles including pure oxides of metals such as Gd, Mn, and Ho can also be explored. If these particles can be synthesized by our bioinspired route and shown to have superior properties including biocompatibility, they can be used for MRI and pathogen detection in foods.

As discussed in Chapter 1, magnetic particles can be used to enhance the contrast in MRI images. MRI contrast enhancement studies can be carried out at the Mary Greeley Medical Center in Ames, IA. Preliminary research can involve some type of tissue in which magnetic

particles can be steered using an MRI scanner that applies external magnetic fields [4]. MRI images can be taken in situ, and contrast enhancement can be observed for different types of magnetic particles. After this preliminary study, animal experiments can be conducted to further show contrast enhancement and to investigate toxicity effects. As discussed in Chapter 1, magnetic particles can be used for the detection of pathogens in foods. GMR sensors that employ magnetic nanoparticles would be a great area of future research because of their high sensitivity to pathogens [5, 6].

Another area of future work involves conjugation of the proteins to the Pluronic. This was done for the cobalt ferrite solution phase studies, and as previously discussed the conjugation had a very positive effect on particle formation [7]. For magnetite synthesis in both solution phase and solid gel phase, future work can involve covalent attachment of the proteins to the Pluronic to study whether conjugation helps in magnetite synthesis.

5.2. References

1. The Protein Research Group, Ohio State University. http://www.biosci.ohio-state.edu/~prg/journalclubs.html (accessed August 16, 2008).

2. Sun, S; Murray, C. B.; Weller, D. K.; Folks, L.; Moser, A. Monodisperse MFe2O4 (M = Fe, Co, Mn) nanoparticles. *Science*. **2000**, 287, 1989–1991.

3. Robinson, D. B.; Persson, H. H. J.; Zeng, H.; Li, G.; Pourmand, N.; Sun, S.; Wang, S. X. DNA-Functionalized MFe2O4 (M) Fe, Co, or Mn) Nanoparticles and Their Hybridization to DNA-Functionalized Surfaces. *Langmuir*. **2005**, 21, 3096-3103.

4. Simonite, T. http://technology.newscientist.com/channel/tech/dn11412-mri-scanner-steers-magnetic-particle-in-live-animals-blood.html. New Scientist Tech. (accessed August 16, 2008).

5. Sandhu, A. New probes offer much faster results. *Nature Nanotechnology*.

2007, 2, 746-748.

6. de Boer, B. M.; Kahlman, J. A. H. M.; Jansen, T. P. G. H.; Duric, H.; Veen, J. An integrated and sensitive detection platform for magneto-resistive biosensors. *Biosens. Bioelectron.* **2007**, 22, 2366–2370.

7. Prozorov, T.; Palo, P.; Wang, L.; Nilsen-Hamilton, M.; Jones, D.; Orr, D.; Mallapragada, S.K.; Narasimhan, B.; Canfield, P.C.; Prozorov, R. Cobalt ferrite nanocrystals: outperforming magnetotactic bacteria. *ACS Nano*. **2007**, 1, 228–233.